JCIM JOURNAL OF CHEMICAL INFORMATION AND MODELING

pubs.acs.org/jcim Article

Structural Assessment of Agonist Efficacy in the μ-Opioid Receptor: Morphine and Fentanyl Elicit Different Activation Patterns

Adrián Ricarte, James A. R. Dalton,* and Jesús Giraldo*

Cite This: J. Chem. Inf. Model. 2021, 61, 1251−1274 Read Online

ACCESS | Metrics & More | Article Recommendations | Supporting Information

ABSTRACT: Over the past two decades, the opioid epidemic in the United States and Canada has evidenced the need for a better understanding of the molecular mechanisms of medications used to fight pain. Morphine and fentanyl are widely used in opiate-mediated analgesia for the treatment of chronic pain. These compounds target the μ-opioid receptor (MOR), a class A G protein-coupled receptor (GPCR). In light of described higher efficacy of fentanyl with respect to morphine, we have performed independent μs-length unbiased molecular dynamics (MD) simulations of MOR complexes with each of these ligands, including the MOR antagonist naltrexone as a negative control. Consequently, MD simulations totaling 58 μs have been conducted to elucidate at the atomic level ligand-specific receptor activity and signal transmission in the MOR. In particular, we have identified stable binding poses of morphine and fentanyl, which interact differently with the MOR. Different ligand−receptor interaction landscapes directly induce sidechain conformational changes of orthosteric pocket residues: Asp149$^{3.32}$, Tyr150$^{3.33}$, Gln126$^{2.60}$, and Lys235$^{5.39}$. The induced conformations determine Asp149$^{3.32}$−Tyr328$^{7.43}$ sidechain−sidechain interactions and Trp295$^{6.48}$−Ala242$^{5.46}$ sidechain−backbone H-bond formations, as well as Met153$^{3.36}$ conformational changes. In addition to differences in ligand binding, different intracellular receptor conformational changes are observed as morphine preferentially activates transmembrane (TM) helices: TM3 and TM5, while fentanyl preferentially activates TM6 and TM7. As conformational changes in TM6 and TM7 are widely described as being the most crucial aspect in GPCR activation, this may contribute to the greater efficacy of fentanyl over morphine. These computationally observed functional differences between fentanyl and morphine may provide new avenues for the design of safer but not weaker opioid drugs because it is desirable to increase the safety of medicines without sacrificing their efficacy.

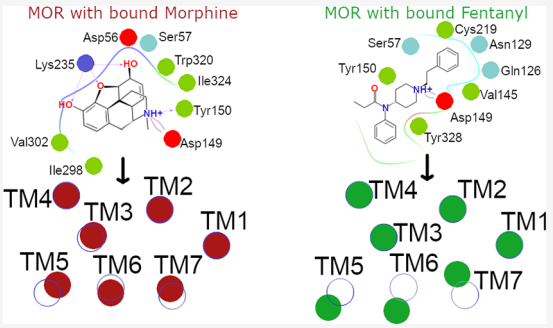

INTRODUCTION

Chronic pain is a major public health problem with a high prevalence and impact on quality of life.[1,2] Opiate-mediated analgesia has shown to be the most efficacious treatment for chronic pain,[3] which primarily targets the μ-opioid receptor (MOR), a class A G protein-coupled receptor (GPCR) encoded by the Oprm1 gene.[4] Upon binding of opioid analgesics, ligand-specific conformational changes occur in the MOR,[5] which lead to activation of the receptor and coupling with intracellular heterotrimeric G_i protein or β-arrestin,[5] thus mediating the propagation of the receptor message through different signaling pathways. It remains elusive precisely how ligand−receptor interactions at the binding site influence MOR conformational dynamics and hence different signal transmissions. While the therapeutic effect of opioid analgesics is mainly attributed to MOR activation through G_i protein signaling,[5−8] their side effects, opioid-induced hyperalgesia, constipation, respiratory depression, and analgesic tolerance, have mostly been linked to β-arrestin signaling.[5−8] Thus, agonists biased toward the G_i protein pathway would be ideal to be considered for drug development as potential future medications. Following this research direction, high expectations were generated by preclinical in vivo studies on the MOR G_i protein-biased agonist TRV130 (oliceridine).[9,10] Oliceridine has been recently approved (August 2020) by the US Food and Drug Administration (FDA) under the trade name Olinvyk for short-term intravenous use in hospitals and other controlled settings.[11] Moreover, in the prescribing information leaflet, it is stated that oliceridine is a full opioid agonist and is relatively selective for the MOR. It is also recognized that, depending on the dose used, adverse reactions, including respiratory, and CNS depression may appear. Importantly, it is also stated that the precise mechanism of the analgesic action is unknown although specific CNS opioid receptors are thought to play a role in the analgesic effects of the drug.[12,13] Thus, although drug discovery programs based on biased agonism seem to be a promising strategy, in particular for the MOR, they still need further

Received: August 5, 2020
Published: January 15, 2021

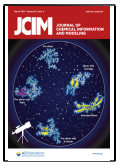

https://dx.doi.org/10.1021/acs.jcim.0c00890
J. Chem. Inf. Model. 2021, 61, 1251−1274

knowledge and experimentation both at the molecular and quantitative pharmacology levels.[14−18] In this regard, following the strategy of MOR biased agonism, several studies have examined how agonists targeting the MOR interact with specific residues to selectively regulate coupling of G_i protein or β-arrestin,[19−23] which in some cases have led to the discovery of new analgesics with reduced negative side effects.[19,24] Yet, although some structural studies of varying MOR agonist efficacy have been addressed,[25,26] there is still a lack of complete understanding of the precise nature of ligand−MOR interactions responsible for observed pharmacological profiles. In this regard, further studies at the atomic level including agonists with different efficacies can shed light on MOR activation mechanisms. This was the reason for selecting morphine and fentanyl for the present study. Fentanyl is a high-efficacy MOR agonist, whereas morphine is a lower-efficacy MOR agonist, which, depending on the assay performed, can behave as a partial agonist.[27,28] It is expected that the generated knowledge can be later incorporated into drug discovery programs addressed to avoid ligands with unwanted effects yet conserving the analgesic capacity of the most powerful drugs.

Biophysical studies of the MOR have led to the determination of three different crystal structures of the receptor: inactive,[29] activated,[5] and fully active[30] structures of the murine MOR (mMOR). In 2012, the inactive crystal structure of the mMOR[29] was obtained by X-ray crystallography, co-crystallized with the morphine-like antagonist β-FNA covalently bound to Lys233$^{5.39}$ (superscript numbers refer to the Ballesteros and Weinstein generic numbering scheme[31]). This structure provided the first high-resolution insight of the MOR,[29] which enabled the application of structure-based computational approaches: rational targeted drug design,[32−34] receptor oligomerization studies with other GPCRs,[35,36] and study of the mechanism by which sodium ions prevent large-scale movement of transmembrane (TM) helix 6 away from TM3, which inhibits receptor activation.[37,38] In 2015, an activated crystal structure of the mMOR bound to the morphine-like agonist BU-72,[5] with intracellular binding of a G protein mimetic camelid antibody fragment (Nb39), was resolved by X-ray crystallography.[5] G protein mimetic nanobodies have been shown to be of great utility for stabilization of active-like states of GPCRs.[39−41] The crystal structure of the activated mMOR shed light on the structural features of MOR activation that are responsible for the efficacy of most therapeutic analgesics. In addition, it allowed the description of an extensive reorganization of the protein−water polar network, required in the full activation process,[5] which is associated with an efficient allosteric coupling between the receptor orthosteric pocket and G_i protein-coupling interface.[5,42] However, it was not until 2018 that a structure of the fully active state of the mMOR was achieved by cryo-electron microscopy.[30] This receptor structure with bound peptide agonist DAMGO and human G_i protein has provided new insights into the mechanism of intracellular binding to the MOR.[30]

Computational techniques such as molecular dynamics (MD) simulations have shown promise in further understanding the complexities of MOR signaling mechanisms. For example, several MD simulation studies of the MOR,[5,7,19,25,26,30] initialized from inactive[29] and activated[5] mMOR crystal structures, have been worthy in assessing some relevant features of the activation process. Briefly, the activated mMOR crystal structure presents, compared to the inactive crystal structure, (i) large outward movement of TM6 relative to TM3, (ii) smaller inward movements of TM5 and TM7, (iii) breakage of the H-bond between Arg165$^{3.50}$ and Thr279$^{6.34}$ (equivalent of the classical Arg$^{3.50}$−Asp/Glu$^{6.30}$ GPCR ionic lock, which involves an acidic amino acid at the position 6.30 that is lacking in the MOR)[43] and formation of a H-bond between Arg165$^{3.50}$ and Tyr252$^{5.58}$, (iv) inward movement of the N$^{7.49}$PxxY$^{7.53}$ motif on TM7 toward TM5,[5,7,19,30] and (v) upward axial movement of TM3.[44] In general, previous MD studies were performed by removing non-native Nb39 and T4 lysozyme, as well as bound ligands BU-72 and β-FNA, from activated and inactive states of the mMOR, respectively.[5,29,30] In particular, a model was provided to show how efficacy depends on small chemical differences in structurally similar morphine-like ligands.[5] A common feature of bound opioid ligands revealed in these studies[5,7,19,29,30,45] is the protonation of their tertiary amine, which is necessary to form a conserved salt bridge with Asp147$^{3.32}$ on TM3 in the orthosteric pocket. This residue is also located within the H-bond distance with Tyr326$^{7.43}$ on TM7 in the mMOR,[46] thus favoring interaction between TM3 and TM7 and activation of the receptor.[44,47−49] This can be observed in activated and inactive crystal structures of the mMOR,[5,29] where the distance between these residues is closer in the activated crystal structure than in the inactive one. In addition, computational studies of the mMOR have reported specific protein−ligand interactions such as the plausible existence of two possible tautomers of His297$^{6.52}$, which can have relevance in ligand function,[19] as well as Tyr326$^{7.43}$ and Gln124$^{2.60}$ H-bonding interactions, which may also determine ligand activity.[6,46] However, computational techniques are yet to satisfactorily explain varying MOR agonist efficacy and potency.

Opioid analgesics, the prototypical pain killers, differ from each other in their structural scaffold and potency. Of all of them, the naturally occurring compound morphine has been considered the reference MOR agonist to which other opioid analgesics are compared.[50] In the last decade, fentanyl, a synthetic opioid 50−100 times more potent than morphine,[51−53] and fentanyl analogs have been related to a rapid increase in the number of opioid overdose deaths because of legal (such as transdermal patches, which led to an increase in deaths up to 2010[54,55]) or illicit manufacture.[51−53,56,57] This has contributed to what is called the opioid epidemic, which has affected mainly the United States and Canada and, in a lower degree, Europe.[58,59] Fentanyl differs from morphine primarily in its pharmacokinetic properties,[50] constituting a highly lipid-soluble drug compared to low lipid solubility of morphine, allowing it to penetrate the blood−brain barrier faster.[50,53] Therefore, fentanyl has a faster onset but shorter duration of action than morphine.[50,53] Following receptor activation, differences in morphine and fentanyl structural scaffolds determine specific ligand-dependent receptor internalization processes.[60] It has been described[60] that high-efficacy opiates like fentanyl induce rapid MOR phosphorylation and internalization compared to morphine. However, 50−100 times potency difference[51−53] between fentanyl and morphine has been widely discussed by in vitro studies[23,61−64] and its potential relation with fentanyl β-arrestin-biased behavior has not been clearly established. In this regard, a recent literature[65] study supports that both fentanyl and morphine work as unbiased agonists[66−68] toward G_i protein and β-arrestin signaling pathways.[61−63] Apparently, contra-

https://dx.doi.org/10.1021/acs.jcim.0c00890
J. Chem. Inf. Model. 2021, 61, 1251−1274

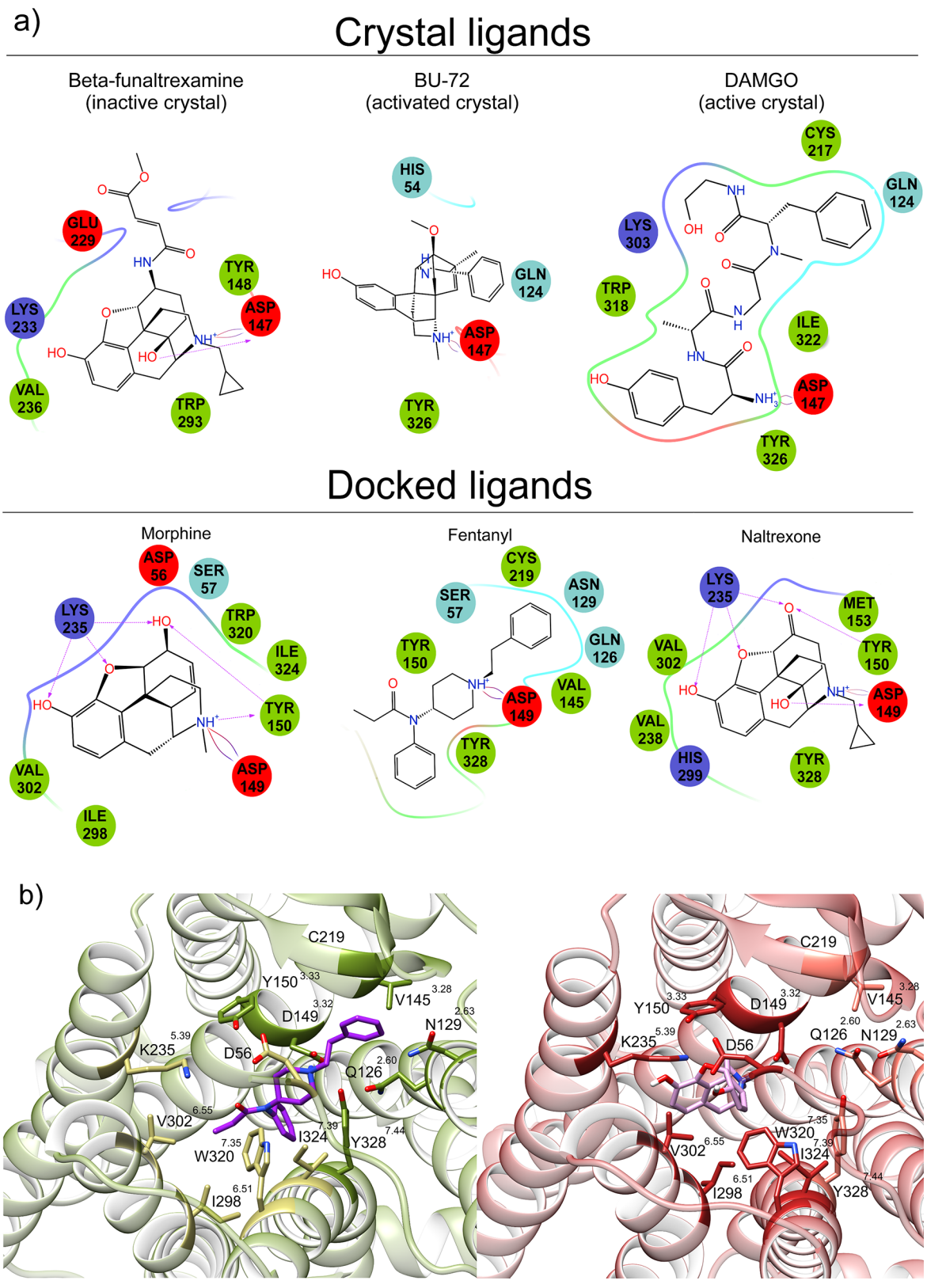

Figure 1. Crystal and docked ligands. Morphine and fentanyl binding poses. (a) 2D binding poses of respective inactive, activated, and fully active co-crystallized ligands: β-FNA, BU-72, and DAMGO, and docked ligands of interest: morphine, fentanyl, and naltrexone. (b) 3D conformation of fentanyl and morphine representative stable binding poses observed during MD simulations (purple and pink, left and right, respectively). Residues of the hMOR in close contact with fentanyl or morphine (<3.5 Å) are colored in dark green or dark red, respectively. Residues colored in light green or light red, respectively, are not in close contact but displayed for comparison purposes.

dictory conclusions on biased signaling may depend not only on the variety of biological assays used but also on the mathematical models and parameters employed. Thus, while the E_{max}/EC_{50} sigmoidal-fitting parameter was chosen in

https://dx.doi.org/10.1021/acs.jcim.0c00890
J. Chem. Inf. Model. 2021, 61, 1251−1274

Vasudevan et al.,[65] a comparison between operational τ/K_A and τ parameters was made in Burgueño et al.[64] In the latter study, while fentanyl was found to be G protein-biased under the τ/K_A parameter, an opposite bias toward the β-arrestin signaling pathway was found when using the τ parameter.[64] Moreover, it has been shown, by measuring the antinociceptive and respiratory depressant effects of some MOR agonists, that the low intrinsic efficacy of some opioid ligands can explain their improved side effect profile.[69] Additionally, a strong correlation between measures of efficacy for receptor activation, G protein coupling, and β-arrestin recruitment was found for some MOR agonists, including those that had previously been described as biased.[69] A detailed review on the relationship between agonist efficacy, biased agonism, and therapeutic window can be bound in Gillis et al.[18]

From the above data, it can be concluded that the mechanisms of MOR activation and signal transduction are not yet fully understood. Although downstream signaling events occur after a number of steps following the initial drug−receptor interactions at the receptor binding site, a chemical connection is expected to be present between initial and final signaling states. Thus, understanding of the distinct receptor conformational changes induced by high- and low-efficacy MOR agonists, and their differential involvement in the activation of the receptor, can be informative to identify the structural features that cause different MOR functionalities. This knowledge is crucial for the rational design of safer but not weaker drugs.

The experimentally observed functional MOR response to morphine and fentanyl is a consequence of molecular events that occur first in the receptor as a result of the interactions established by these ligands with residues of the receptor binding pocket, which are then transmitted from the extracellular to the intracellular side of the cell membrane. In this context, in the present study, we performed unbiased μs-length MD simulations to complete a detailed atomic-level study of the receptor conformational space induced or selected in the MOR by morphine and fentanyl in order to explain the variations seen in opiate efficacy.[27] Receptor activation by either induction or selection of receptor active states has been recurrently under debate[70] though they may coexist and be part of the same thermodynamic cycle.[71] Here, both models are considered, which will allow noteworthy structural comparisons. In order to understand how opioid analgesics transmit their molecular signal and generate effects in humans, we consider it appropriate to perform our study in the native human MOR (hMOR) and across multiple independent MD trajectories. Our results show that fentanyl displays a completely different binding pose from morphine, which leads to divergent effects on the orthosteric pocket conformational arrangement. The fact that both morphine and fentanyl could activate both G_i protein and β-arrestin signaling pathways raises the question of which signaling pathway corresponds to the receptor conformational changes found computationally. This is a question for which there is not a definite answer with the present knowledge. Nevertheless, to avoid speculations, structural comparison of computational structures was made with the current MOR crystal structures,[5,29,30] which are related to the G_i signaling pathway. Our results show that extracellular conformational changes of the receptor compromise the ability of its intracellular side to consistently reach (induce) or maintain (select) the G_i protein-signaling fully active state.[30]

RESULTS

Homology Models of the hMOR Remain Conformationally Stable in Control MD Simulations. Native activated and inactive hMOR homology models were generated from respective activated and inactive mMOR crystals[5,29] by renumbering sequences, mutating non-conserved residues, and adding non-crystallized segments of the inactive hMOR N-terminus, inactive hMOR intracellular loop, and activated hMOR C-terminus (see Methods). In order to validate the accuracy of activated and inactive hMOR models, we performed two control replicas of 2 μs-length unbiased MD simulations with co-crystallized agonist BU-72[5] and three control replicas of 3 μs-length with docked antagonist naltrexone, respectively. As co-crystallized antagonist β-FNA of the inactive mMOR[29] is covalently bound to Lys233$^{5.39}$, it is not an ideal control antagonist for our purposes here, but because of high similarity between the molecular structures of naltrexone and β-FNA (Figure 1), β-FNA can be easily substituted for naltrexone. Therefore, in order to test docking accuracy, BU-72 was re-docked into our hMOR active model, while naltrexone was docked into our inactive hMOR model and compared to co-crystallized β-FNA. Docking results reveal a top-ranked BU-72 binding pose with a root mean square deviation (RMSD) of 0.4 Å from its co-crystallized position and a top-ranked naltrexone binding pose with an RMSD of 0.7 Å compared to the common heavy atoms of co-crystallized β-FNA. Trajectories of the hMOR with bound BU-72 and naltrexone show stable receptor conformations (average RMSDs of 1.8 Å (0.4 SD) and 2.8 Å (0.2 SD), respectively (Figures S1 and S4)) and ligand binding poses (average RMSDs of 1.7 Å (0.6 SD) and 2.2 Å (0.6 SD), respectively (Figures S1 and S2)). These results indicate that both activated and inactive hMOR models remain near their initial conformation throughout long-timescale MD trajectories, which supports their use as reliable starting points to evaluate the binding effect of ligands of interest: morphine and fentanyl.

Binding Poses of Morphine and Fentanyl Differ. In order to computationally examine at the atomic level the MOR efficacy differences between fentanyl and morphine, we first docked each ligand into our models of activated and inactive hMOR models. Starting from these protein−ligand systems, we performed three replicas of 3 μs-length unbiased MD simulations to allow for ligand-dependent receptor conformational change. From the respective morphine- and fentanyl-bound MD trajectories, we identified one stable binding pose for each ligand (Figure 1), consistent across all replicas and predominantly selected over other alternative temporary poses (Figure S2). According to RMSD across MD simulations (Figure S2), and considering a threshold of ± 2.5 Å to define ligand stability, we observe that both morphine and fentanyl are stable after the first microsecond of simulation time and until the end of each trajectory, independently of the initial receptor state (average ligand RMSDs of 1.3 Å (0.5 SD) and 2.2 Å (0.5 SD), respectively). Notable initial ligand instability, limited to the first microsecond of replicas starting from the receptor activated state with bound fentanyl and replicas #1 and #2 starting from the receptor inactive state with bound morphine, can be explained by receptor−ligand relaxation and adaptation (Figure S2). Therefore, both ligands are bound in a stable fashion, and any differences in ligand stability in the activated state are probably a result of better fit of the mMOR crystal structure for morphine-like ligands, as well as

https://dx.doi.org/10.1021/acs.jcim.0c00890
J. Chem. Inf. Model. 2021, 61, 1251−1274

differences in the molecular scaffold between morphine and fentanyl (Figure 1). On the other hand, difference of size between co-crystallized morphine-like ligands of activated[5] and inactive[29] mMOR models, BU-72 (smaller) and β-FNA (larger), respectively, creates a wider orthosteric pocket in the inactive hMOR model. This may allow ligands larger than morphine, like fentanyl, to obtain its preferred binding pose faster in this receptor state. Nevertheless, irrespective of initial receptor conformation, both morphine and fentanyl reach consistent stable poses in the orthosteric pocket over replicated trajectories, which indicate satisfactory docking accuracy (Figure 1).

Differences are not only observed in the conformation of morphine and fentanyl but also in orthosteric pocket residues that are in close contact with them (ligand−residue distance <3.5 Å). The distribution of residues most frequently making contact, summarized in Table 1, indicates that morphine establishes its most stable interactions with the N-terminus, extracellular regions of TM helix 5, TM6, and TM7, and a section of TM3 facing TM5 (Figure 1 and Figure S3). On the other hand, fentanyl establishes more frequent contact with extracellular loop (ECL) 2, extracellular regions of TM2 and TM7, and a section of TM3 facing TM2 (Figure 1 and Figure S3). Interestingly, fentanyl comes into contact with $Cys219^{ECL2}$, which is directly involved in an important structural disulfide bond with $Cys142^{3.25}$, which may have implications for conformational change in TM3,[72] especially as this helix has previously been described to undergo an upward axial movement in receptor activation of class A GPCRs.[44,73] In addition to fentanyl and morphine, in the present study, we have performed three additional replicas of 3 μs-length unbiased MD simulations with the MOR-bound antagonist naltrexone starting from the activated hMOR state, which supports the comparison between morphine and fentanyl. Naltrexone, similar to morphine and fentanyl, overall maintains a stable disposition in the binding pocket across replicas (Figure S2). However, when compared to control replicas where naltrexone is bound in the inactive hMOR state, it presents a slightly worse receptor accommodation (average RMSDs of 2.6 Å compared to 2.2 Å, Figure S2) as might be expected for its antagonist condition. Similarities between naltrexone and morphine scaffolds lead to similar interaction environments (Figure 1 and Table 1). Thus, contact between naltrexone and the hMOR is similarly and frequently formed with TM5, TM6, TM7, and a section of TM3 facing TM5 (Table 1 and Figure S3). However, differently from morphine, naltrexone comes into close contact with $Tyr328^{7.43}$, a residue also involved in the interaction between fentanyl and the receptor in our MD simulations. As these interactions with $Tyr328^{7.43}$ are common to both a potent agonist and an antagonist, it could be speculated that they are apparently associated with affinity rather than with efficacy. However, a detailed analysis of the simulations reveals a fine structural tuning of this residue, which allows the functional distinction between agonists and antagonists (see below).

Table 1. Crystal Ligands, Morphine, Fentanyl, and Naltrexone Protein−Ligand interactions[a]

ligand	unique interactions		common interactions	
crystal ligands				
beta-funaltrexamine (inactive crystal)	$mTyr148^{3.33}$		$mAsp147^{3.32}$	
	$mGlu229^{5.35}$			
	$mLys233^{5.39}$			
	$mVal236^{5.42}$			
	$mTrp293^{6.48}$			
BU-72 (activated crystal)	$mPro59^{N\text{-}ter}$		$mAsp147^{3.32}$	
	$mLeu129^{2.65}$		$mTyr326^{7.43}$	
DAMGO (active crystal)	$mGln124^{2.60}$		$mAsp147^{3.32}$	
	$mCys217^{ECL2}$		$mTyr326^{7.43}$	
	$mLys303^{6.58}$			
	$mTrp318^{7.35}$			
	$mIle322^{7.39}$			
docked ligands				
morphine	$hAsp56^{N\text{-}term}$		$hSer57^{N\text{-}term}$	
	$hLys235^{5.39}$	(i)	$hAsp149^{3.32}$	(i) (ii) (iii)
	$hIle298^{6.51}$		$hTyr150^{3.33}$	(i)
	$hVal302^{6.55}$			
	$hTrp320^{7.35}$	(iii)		
	$hIle324^{7.39}$			
fentanyl	$hGln126^{2.60}$	(iii)	$hSer57^{N\text{-}term}$	
	$hAsn129^{2.63}$		$hAsp149^{3.32}$	(i) (ii) (iii)
	$hVal145^{3.28}$		$hTyr150^{3.33}$	(i)
	$hCys219^{ECL2}$	(iii)		
	$hTyr328^{7.43}$	(ii) (iii)		
naltrexone	$hMet153^{3.36}$		$hAsp149^{3.32}$	(i) (ii) (iii)
	$hLys235^{5.39}$	(i)	$hTyr150^{3.33}$	(i)
	$hVal238^{5.42}$	(i)		
	$hHis299^{6.52}$			
	$hVal302^{6.55}$			
	$hTyr328^{7.43}$	(ii) (iii)		

[a]Residues in close contact (<3.5 Å) listed with respective murine (m) or human (h) numbering following the Ballesteros and Weinstein generic scheme,[31] for crystal structures and MD systems, respectively. Residues interacting with morphine, fentanyl, and naltrexone are included when frequency of contact is >20% of trajectory time during at least two MD simulation replicas, independent of the initial state of the receptor. Similarity between residues in contact across crystals and MD simulations are labeled as common to the (i) inactive crystal, (ii) activated crystal, and (iii) fully active crystal.

Fentanyl and Morphine Induce Different Receptor Activation Pathways. According to RMSD of the transmembrane domain (TMD), the hMOR experiences varying degrees of backbone conformational change across our MD simulations (Table S1 and Figure S4). This is an expected result as the MOR is known to be a highly dynamic protein,[5,7,29,30] as shown when comparing both activated and inactive crystals[5,29] with the fully active crystal structure[30] (TMD RMSDs of 1.4 and 3.0 Å, respectively). Making use of a threshold of ± 3.5 Å, calculated from TMD RMSD of crystal structures, we quantified the conformational changes between active and inactive states with respect to either its initial state or fully active crystal. In general terms, receptor conformation is relatively stable (≤ 3.5 Å) in all replicas starting from the activated state with the bound agonist (morphine or fentanyl) with an average TMD RMSD of 3.2 Å (0.4 SD) from its initial state and 2.2 Å (0.4 SD) from the fully active crystal[30] (Table S1 and Figure S4). On the contrary, in MD simulations starting from the inactive state with the bound agonist (morphine or fentanyl), TMD conformations remain mostly inactive-like with an average TMD RMSD of 2.8 Å (0.3 SD) from its initial state and distant (> 3.5 Å) from the fully active crystal[30] (TMD RMSD of 3.6 Å (0.4 SD), Table S1 and Figure S4). However, the receptor in replicas #2 and #3 with bound fentanyl or replica #2 with bound morphine starting from the

https://dx.doi.org/10.1021/acs.jcim.0c00890
J. Chem. Inf. Model. 2021, 61, 1251−1274

inactive state presents occasional TMD RMSDs of 2.8 and 2.9 Å or 2.6 Å from the fully active crystal,[30] respectively, which indicate transient receptor activation toward active-like states (≤3.5 Å, Figure S4). Larger conformational changes in simulations starting from the activated state than those starting from the inactive state are explained by the lack of the intracellular partner in our models. In more detail, computational results also suggest that both activated and inactive crystal structures[5,29] (and the models generated from them) are better adapted to morphine than fentanyl because of the similarity between morphine and the co-crystallized ligand scaffolds, which implies that the receptor has to undergo bigger conformational changes to properly bind fentanyl. TMD conformational changes can be compared with those observed when the antagonist naltrexone is bound, where a clear tendency toward inactivation is observed when starting from the activated state (average RMSD of 3.9 Å (0.3 SD) from the initial state, Table S1) and a preservation of the inactive state is found in control replicas starting from the inactive state (average RMSD of 2.8 Å (0.2 SD) from the initial state, Table S1). Surprisingly, when comparing naltrexone-bound receptor simulations with the fully active crystal,[30] the average RMSD achieved is only 3.0 Å (0.4 SD) or 3.7 Å (0.3 SD) in trajectories starting from activated or inactive states, respectively (Table S1). In order to better describe receptor intracellular conformational changes involved in receptor activation, four metrics were employed relative to the protein center, considering only the two last microseconds of MD simulations: (i) TM3, which moves upward, (ii) intracellular tips of TM5 and (iii) TM6, which move inward and outward, respectively; and (iv) NPxxY motif of TM7,[43] which rotates toward the core of the helical bundle. Meanwhile, a fifth metric was used for assessing intracellular separation between TM3 and TM6: the distance between residues Arg167$^{3.50}$ and Thr281$^{6.34}$ (Arg−Thr), which is equivalent to the ionic lock in class A GPCRs.[43,74−76] Thresholds for these metrics were based on fully active,[30] activated,[5] and inactive[29] crystal structures (normalized according to the inactive crystal structure), with a representative sign, which represents the movement involved with respect to the receptor center (inward or outward movement, or downward or upward movement, "−" or "+" sign, respectively): +0.3 Å for TM3, −0.8 Å for TM5 and NPxxY, +1.7 Å for TM6, and + 10.0 Å for Arg−Thr distance as utilized in a previous study.[7] These thresholds were fine-tuned with naltrexone-bound MD simulation results to classify active- or inactive-like conformations of the five intracellular metrics.

Upward axial movement of TM3 (Figures 2 and 3, Table S1, and Figure S5) is a key indicator of receptor activation, as shown previously in other GPCRs.[77,78] Comparison between mMOR crystal structures shows that TM3 adopts a more upward position when the receptor is activated: by distances of +0.2 Å and +0.6 Å in activated[5] and fully active[30] crystals with respect to the inactive one,[29] respectively. Based on these differences and antagonist-bound MD simulations (average movement of +0.1 Å (0.2 SD) and + 0.3 Å (0.2 SD) in replicas starting from activated or inactive states, respectively), we considered a threshold value of +0.3 Å. Our trajectories show that replicas #2 and #3 starting from the activated hMOR with bound fentanyl present an average TM3 upward axial movement of +0.6 Å (0.2 SD), more upward than the initial receptor activated state and adopting a conformation similar to the fully active crystal[30] (Figure 3, Table S1, and Figure S5). In

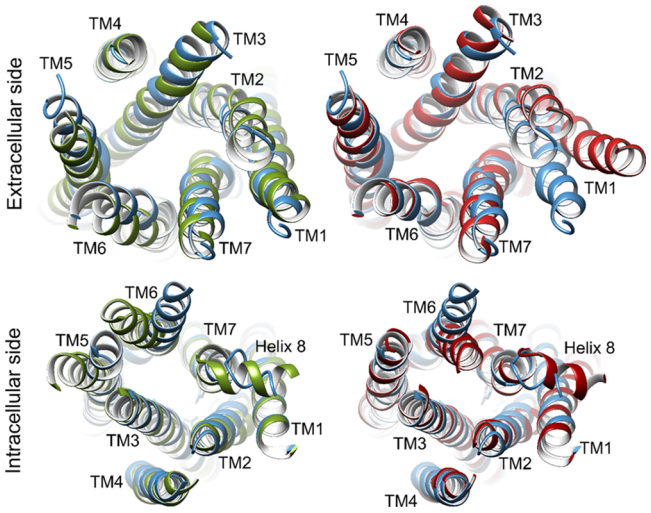

Figure 2. Conformational change of the TM domain in MD simulations of the inactive hMOR. Extracellular (top) or intracellular (bottom) views of representative receptor conformations from replicas #3 and #1 starting from the inactive state with bound fentanyl (left, in green) or morphine (right, in red), respectively, compared with the fully active crystal structure (blue).

replica #1, the receptor maintains an average active-like position of +0.3 Å (0.2 SD, Figure 3, Table S1, and Figure S5). In comparison, all replicas starting from the activated state with bound morphine, despite transient active-like TM3 conformations, show an average less active-like TM3 position of only +0.2 Å (0.2 SD, Figure 3, Table S1, and Figure S5). Surprisingly, the tendency observed in replicas starting from the activated state, where fentanyl selects for more upward conformations of TM3 than morphine, is not conserved in replicas starting from the inactive hMOR. Under this condition, 2/3 trajectories with bound morphine (replicas #1 and #3) induce an active-like average shift of +0.3 Å (0.2 SD), while replica #2 shows an even larger average of +0.6 Å (0.2 SD), in accordance with the fully active crystal[30] (Figure 3, Table S1, and Figure S5). On the contrary, none of the replicas starting from the inactive state with bound fentanyl presents average TM3 movements ≥ +0.3 Å, resulting in mostly selecting an inactive-like TM3 conformation (Figure 3, Table S1, and Figure S5). Interestingly, under these conditions, replica #3 shows a downward TM3 movement of −0.4 Å (0.2 SD, Figure 3, Table S1, and Figure S5), which suggests that the specific contact fentanyl establishes with Cys219^{ECL2} does not reliably invoke TM3 upward axial movement, at least when starting from the inactive state. Rather, direct interactions between the ligand and TM3 appear more influential, as evidenced by the more numerous interactions morphine makes with TM3 relative to fentanyl. In terms of other TM helices, the distance between the protein center and intracellular tip of TM5 (see Methods) decreases in activated[5] or fully active crystal structures[30] with respect to the inactive structure[29] by −1.5 Å or −2.1 Å, respectively. Considering these crystal movements and naltrexone-bound MD simulations (average movement of +0.5 Å (0.6 SD) and +0.2 Å (0.5 SD) in replicas starting from activated or inactive states, respectively), a threshold of −0.8 Å can therefore be established for determining active- or inactive-like conformations of TM5. In MD simulations starting from the activated hMOR with either fentanyl or morphine bound, as expected, TM5 stabilizes

https://dx.doi.org/10.1021/acs.jcim.0c00890
J. Chem. Inf. Model. 2021, 61, 1251−1274

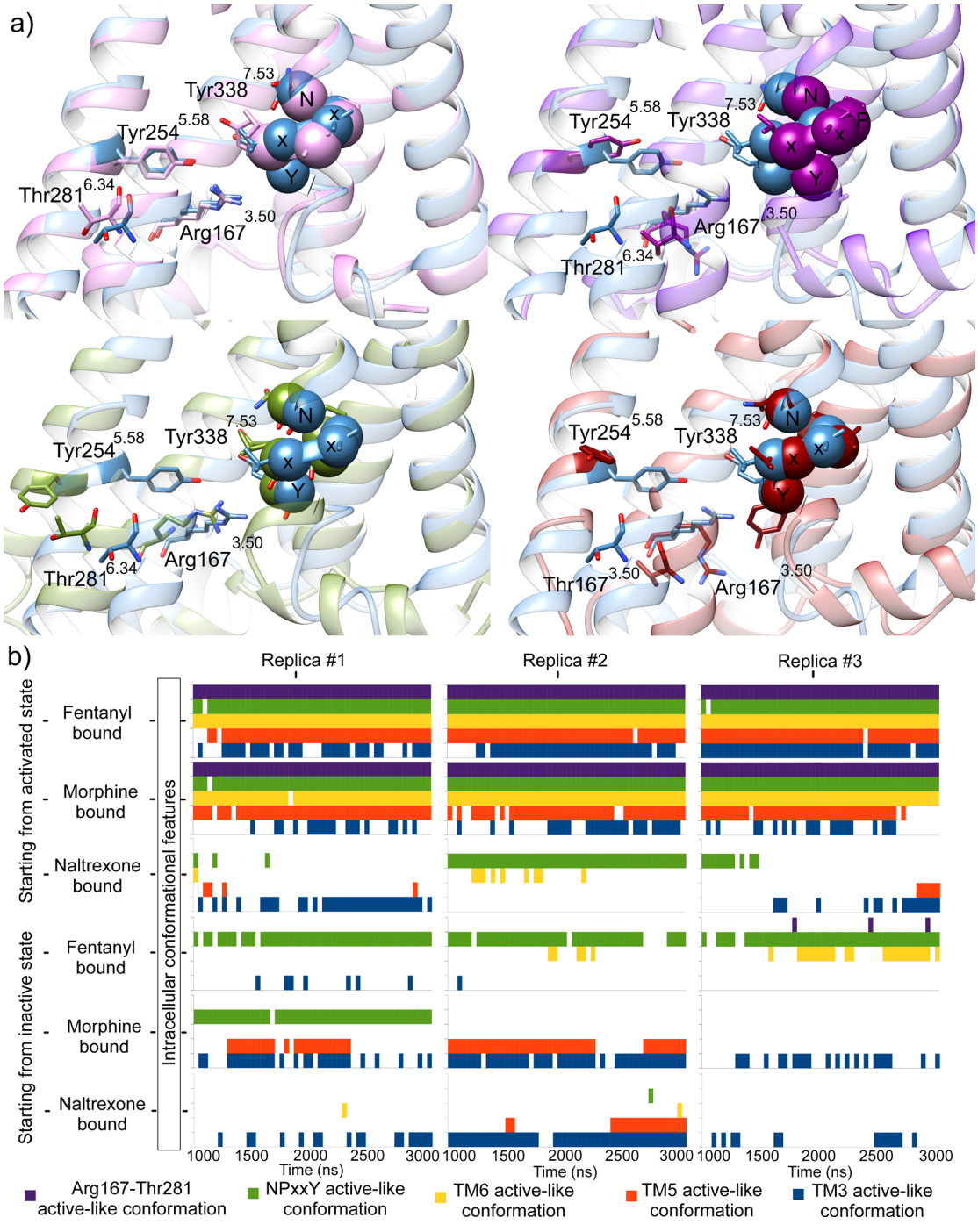

Figure 3. Intracellular conformation in MD replicas defined by the Arg167$^{3.50}$–Thr281$^{6.34}$ distance, vertical TM3 movement, and lateral NPxxY motif, TM5, and TM6 movements. (a) Structural comparison between the fully active crystal[30] (blue) and either activated[5] or inactive[29] crystals (top, pink or purple, left or right, respectively), or representative conformation of MD-generated replicas #3 and #1 starting from the inactive state with bound fentanyl or morphine, respectively (bottom, green or red, left or right, respectively). As a function of time, (b) active- or inactive-like states of the five different activation-related intracellular features of each replica starting from the activated or inactive hMOR with bound fentanyl, morphine, or naltrexone (active-like conformations of: Arg167$^{3.50}$–Thr281$^{6.34}$, NPxxY, intracellular TM6, intracellular TM5, and TM3, in purple, green, yellow, orange, or blue, respectively). White gaps represent inactive-like conformations of each respective metric. See the Methods section for thresholds used to define active- or inactive-like states of intracellular features and Figure S5,S6 for respective metric individual time-dependent analysis.

(selects) the active-like conformation with normalized distances mostly between −0.8 Å and − 2.1 Å (Figure 3, Table S1, and Figure S5). An exception is replica #3 with bound morphine, where TM5 fails to reliably select an active-like conformation and instead permits a change toward an inactive-like conformation with a maximum of +0.7 Å at 2.8 μs (Figure S5). Likewise, in trajectories starting from the inactive state with bound fentanyl or morphine, TM5 does not obtain an active-like conformation and remains inactive (Figure 3, Table S1, and Figure S5). Moreover, in replica #3, TM5 undergoes an average change of +1.7 Å with a maximum of +2.9 Å (Figure S5), which places TM5 in a more outward

https://dx.doi.org/10.1021/acs.jcim.0c00890
J. Chem. Inf. Model. 2021, 61, 1251−1274

conformation with respect to the receptor core (Figures 2 and 3, Table S1, and Figure S5). This may be the result of an outward movement of TM6 (see below), which temporarily influences TM5 through their mutual interhelical contact, an effect observed in active-like crystal structures.[5,30] Exceptionally, replicas #1 and #2 when morphine is bound in MD simulations starting from the inactive state present transient or sustained inward TM5 movement induction with maximum and average displacements of −1.7 Å and −1.5 Å (0.8 SD), respectively (Figure S5). Altogether, these results indicate that TM5 generally remains in an active-like conformation if the receptor begins in that state, or if initially inactive, morphine is more effective than fentanyl at inducing active-like conformations of TM5 (Figures 2 and 3, Table S1, and Figure S5). Similarly, activated[5] and fully active[30] crystal structures present a more outward TM6 intracellular tip conformation (see Methods) relative to the inactive crystal,[29] with TM6 respectively moving +2.1 Å and +2.0 Å away from the protein center. Based on these differences and naltrexone-bound MD simulations (average movement of +0.8 Å (0.5 SD) and +0.6 Å (0.4 SD) in replicas starting from activated or inactive states, respectively), a distance threshold of +1.7 Å can therefore be used for defining active- or inactive-like conformations of TM6. This helix selects an active-like outward conformation with an average distance of +3.5 Å (0.6 SD) in trajectories starting from the activated hMOR, independent of the agonist bound (Figure 3, Table S1, and Figure S6). However, a transient deactivation of TM6 occurs when it falls into an inactive-like conformation in replica #1 with bound morphine at 1.8 μs, recording a distance of +1.4 Å (Figure S6). Likewise, in all replicas starting from the inactive hMOR with bound morphine, TM6 does not demonstrate any outward movement, maintaining only an average distance of +0.4 Å (0.4 SD) with respect to the inactive crystal and below the +1.7 threshold (Figure 3, Table S1, and Figure S6). However, with bound fentanyl, active-like conformations of TM6 are induced in replicas #2 and #3 with maximum values of +2.3 Å and +3.2 Å, respectively (Figures 2 and 3, Table S1, and Figure S6). While in replica #2 these conformational changes are observed transiently, a more sustained conformational change occurs in replica #3 with an average TM6 movement of +1.9 Å (0.6 SD) over the last microsecond. Altogether, these results indicate that while both fentanyl and morphine are able to select an active-like conformation of TM6 in simulations starting from the activated state, uniquely fentanyl is able to induce TM6 activation when starting from the inactive state, which leads TM6 to adopt conformations more similar to activated and fully active crystals[5,30] (Figures 2 and 3, Table S1, and Figure S6). This may represent an indication of the greater efficacy of fentanyl relative to morphine.

Rearrangement of TM helices during receptor activation leads to specific intracellular conformational changes such as the NPxxY motif on TM7 and Arg167$^{3.50}$−Thr281$^{6.34}$ interaction (Figure 3). The fully active crystal structure of the mMOR[30] allows a better understanding of the conformational changes adopted by these regions when the intracellular G_i protein partner is bound to the receptor. Interestingly, in the fully active crystal,[30] the NPxxY motif adopts an alternative conformation closer to the inactive crystal structure[29] than to the activated crystal structure.[5] This difference may be due to the non-native binding of Nb39 to the receptor. In these crystal structures, the NPxxY position can be described according to the protein center. As such, activated[5] and fully active[30] crystals present more inward positions of the NPxxY motif than the inactive crystal[29] (−1.7 and −0.8 Å, respectively). Consequently, in addition to antagonist-bound MD simulations (average movement of −0.8 Å (0.6 SD) and +0.1 Å (0.3 SD) in replicas starting from activated or inactive states, respectively), a threshold of −0.8 Å can be defined and applied for determining active- or inactive-like conformations of this intracellular region (Figure 3, Table S1, and Figure S6). Because of computational limitations, our MD simulations do not include bound G_i protein; therefore, it might be expected that activated-like NPxxY conformations could be selected or induced over fully active conformations. During MD simulations starting from the activated state, NPxxY is broadly selected in its original conformation with an average distance of −2.5 Å (0.5 SD), independent of the agonist bound (Figure 3, Table S1, and Figure S6). On the other hand, all replicas starting from the inactive state with bound fentanyl induce a conformational change so that NPxxY achieves a stable active-like position (average of −1.4 Å, 0.6 SD), which is the greatest in replica #3 (average of −1.8 Å, 0.7 SD, Figure 3, Table S1, and Figure S6). Conversely, when morphine is bound, only replica #1 starting from the inactive state induces an active-like position that crosses the −0.8 Å threshold (average of −1.5 Å, 0.3 SD, Figure S6), whereas other replicas select an inactive-like conformation. These results suggest that fentanyl consistently induces active-like conformations of both TM7 and the NPxxY motif stronger than morphine (Figure 3). The intracellular distance between Arg167$^{3.50}$ and Thr281$^{6.34}$, equivalent to the ionic lock in class A GPCRs,[43,74−76] can be classified as being in an active- or inactive-like conformation by applying a threshold value of +10.0 Å, as used previously.[7] The Arg−Thr distance is broadly selected in its original state in respective MD simulations starting from activated or inactive states, independent of the agonist bound, resulting in respective averages of 13.0 Å (0.9 SD) and 6.5 Å (0.5 SD, Figure 3, Table S1, and Figure S7). However, in replica #3 when starting from the inactive state with bound fentanyl, this interaction is seen to transiently break at 1.8 μs when the distance reaches 10.1 Å (Figure S7). In the replicas where naltrexone is bound, Arg167$^{3.50}$ and Thr281$^{6.34}$ reach and stabilize distances <10 Å over the entire two last microseconds of MD simulations, started from either control inactive or activated states, as expected by the antagonist nature of naltrexone, contrary to the overall active-like states selected by agonists when starting from the activated state (Figure 3, Table S1, and Figure S7). Similarly, naltrexone induces an inward movement of TM6, in parallel to an outward movement of TM5 and the NPxxY region, in simulations starting from the activated state, thus adopting, as expected, inactive-like conformations of these metrics (Figure 3, Table S1, and Figure S7). This result indicates that the threshold used clearly differentiates between active- or inactive-like states of this interaction. Altogether our results strongly indicate that receptor activation by means of TM6 outward movement (Figures 2 and 3, Table S1, and Figure S5-S7) is more frequently observed with bound fentanyl, which is uniquely able to initiate in a μs time period, than with morphine. Therefore, in addition to conformational changes of helical regions mentioned above, the different frequency of activation of these intracellular metrics is consistent with the experimentally observed difference in efficacy between morphine and fentanyl.

https://dx.doi.org/10.1021/acs.jcim.0c00890
J. Chem. Inf. Model. 2021, 61, 1251−1274

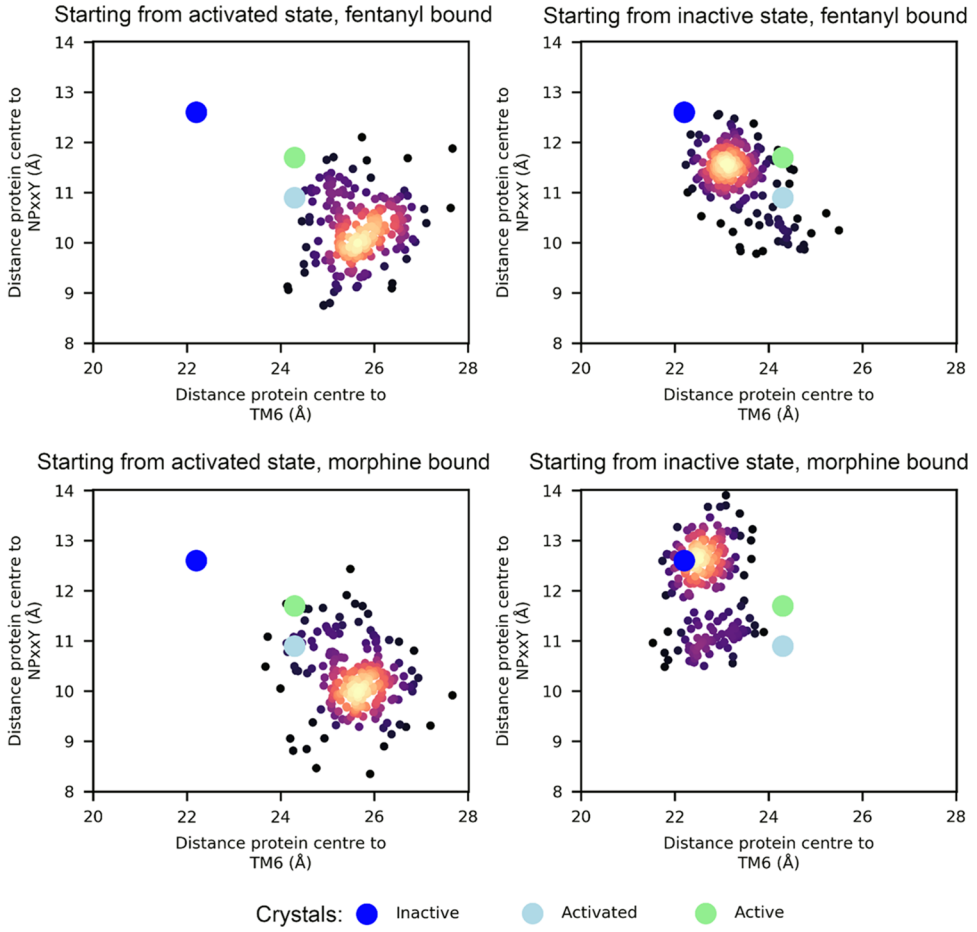

Figure 4. Density maps of the outward movement of TM6 and conformation of the NPxxY motif with respect to the protein center. Density maps of fentanyl or morphine (top or bottom row, respectively) of the three replicas started from activated or inactive states (left or right column, respectively). Inactive, activated, and fully active crystals are represented for comparison by dark blue, light blue, or green, respectively. Density maps show conformations more or less frequently induced represented with a hot to cold color gradient.

All these TMs and intracellular metric movements (average tendencies summarized in Table S1) observed during receptor (in)activation are indicative of conformational changes at the intracellular side of the receptor in system dynamics starting either from activated or inactive states. As shown in Figure 3, some of these activation features co-exist in time. Therefore, their simultaneous presence represents a highly active conformation of the receptor. However, the activation of one feature prior to another can be an indication of the exploration of a certain process or pathway of receptor activation. Our results indicate that all active-like conformational intracellular metrics are mostly preserved in MD simulations starting from the activated agonist-bound receptor state, which is biologically reasonable because morphine and fentanyl are both agonists. However, agonist-specific differences are consistently observed during receptor activation from the inactive state. While with bound morphine, the hMOR largely presents an upward axial movement of TM3 and exclusively induced TM5 active-like conformations, with bound fentanyl, the hMOR shows specific activation of TM6 and stronger activation of the NPxxY motif on TM7 (Figure 3). Interestingly, replica #3 starting from the inactive state with bound fentanyl, which most frequently presents active-like conformations of TM6 and the NPxxY motif, is the only replica that yields transient active-like Arg167$^{3.50}$–Thr281$^{6.34}$ distances (Figure 3). The non-preservation of this Arg167$^{3.50}$–Thr281$^{6.34}$ separation may be a result of the absence of TM3 upward axial movement, which, in addition to TM6 outward movement, is required to properly break intracellular TM3–TM6 interactions. Altogether, these results are indicative of different receptor activation pathways induced by morphine (TM3 and TM5) and fentanyl (TM6 and TM7).

It has been widely discussed if fentanyl acts as a β-arrestin biased agonist or behaves as a balanced agonist.[18,23,61−68] As done for other GPCRs,[77,78] we performed a density map (Figure 4) of the receptor intracellular state achieved considering two of the main representative intracellular metrics, which conformationally differ more between morphine and fentanyl: (i) outward movement of the intracellular side of TM6 and (ii) conformation of NPxxY with respect to the protein center. This representation (Figure 4) suggests that in our MD simulations, we reach a common active-like state with either fentanyl or morphine bound. It should be considered that our models starting from the activated hMOR were modeled from its respective crystal,[5] which contains a G protein mimetic camelid nanobody subsequently removed in our model. Therefore, the conformations achieved in our trajectories can be conditioned by the initial crystal used, which may limit the observations of other alternative conformations. However, in a timescale of three microseconds, our simulations have not identified receptor conformational regions consistent with biased agonism, in agreement with a

https://dx.doi.org/10.1021/acs.jcim.0c00890
J. Chem. Inf. Model. 2021, 61, 1251−1274

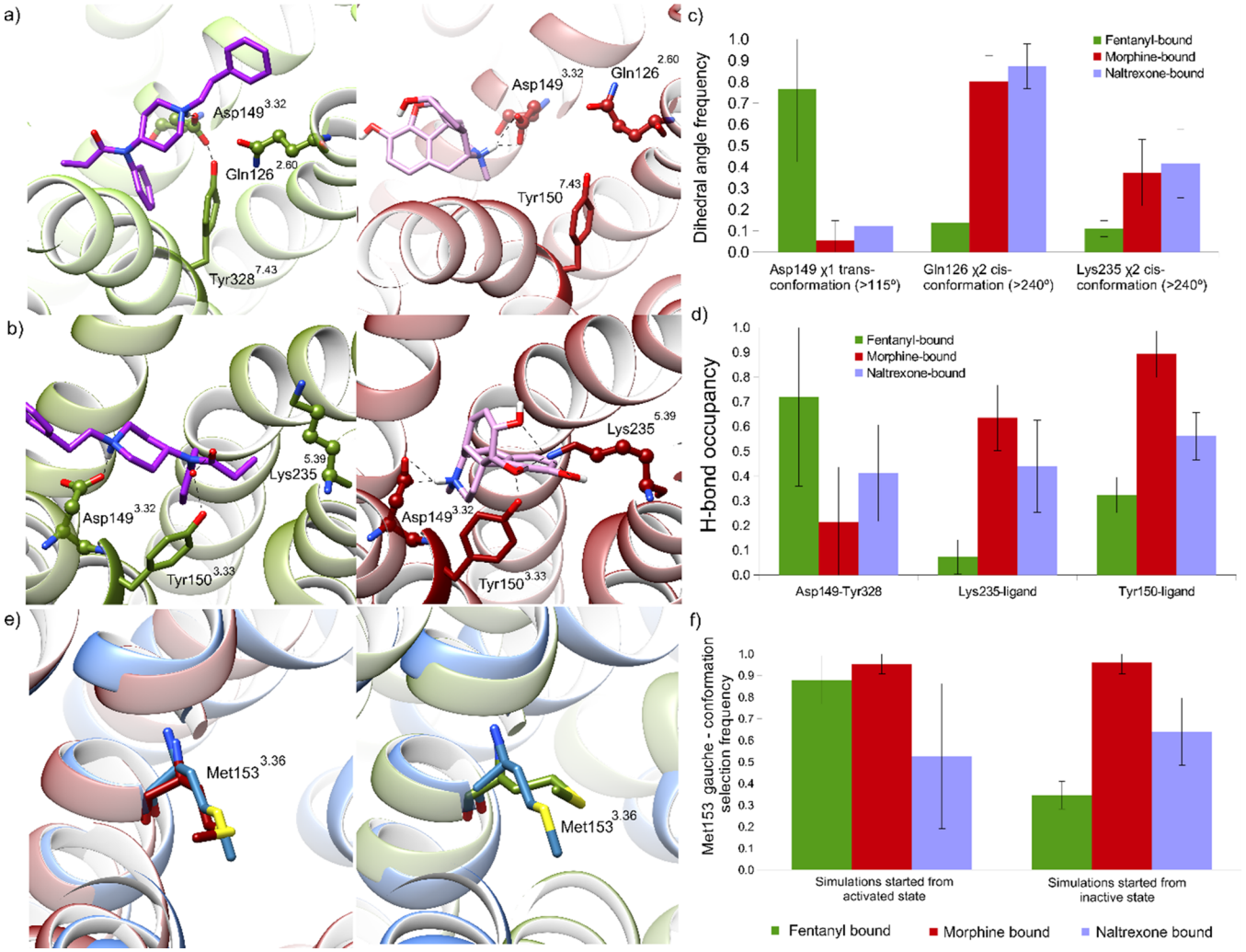

Figure 5. Orthosteric pocket conformational changes of the hMOR in MD simulations. (a) and (b) Predominant *trans* (~180.0°) or *cis* conformation (~300.0°) of (a) Gln126$^{2.60}$ χ2 dihedral angle or (b) Lys235$^{5.39}$ χ2 dihedral angle, in representative MD conformations with bound fentanyl or morphine (purple or pink, hMOR residues in green or red, left and right, respectively). Structural images also show different Asp149$^{3.32}$ χ1 dihedral angle *cis* and *trans* conformations selected, and Asp149$^{3.32}$–ligand, Tyr150$^{3.33}$–ligand, or Asp149$^{3.32}$–Tyr328$^{7.43}$ H-bond formation. (c) Conformation frequency of the Asp149$^{3.32}$ *trans* χ1 dihedral angle or Gln126$^{2.60}$ and Lys235$^{5.39}$ *cis* χ2 dihedral angle selected with bound fentanyl, morphine, or naltrexone, independent of the initial state of the receptor (green, red, or purple, respectively). (d) H-bond occupancy of Asp149$^{3.32}$–Tyr328$^{7.43}$, Lys235$^{5.39}$–ligand, or Tyr150$^{3.33}$–ligand interaction of simulations with bound fentanyl, morphine, or naltrexone, independent of the initial state of the receptor (green, red, or purple, respectively). (e) Structural comparison of Met153$^{3.36}$ conformation between the fully active crystal[30] (blue) and either replica #3 starting from the inactive state with bound morphine or fentanyl (red or green, left or right, respectively). (f) Frequency of Met153$^{3.36}$ *gauche*− conformation in trajectories with bound fentanyl, morphine, or naltrexone, starting from activated or inactive states (green, red, or purple, respectively).

recent experimental study.[65] It is worth noting that conclusions on biased agonism from experimental functional studies may depend on the parameter used for its quantification, where the proposed $\Delta\Delta\log(\tau/K_A)$, $\Delta\Delta\log(\tau)$, or $\Delta\Delta\log(E_{max}/EC_{50})$ bias factors have led to different biased profiles when applied to fentanyl, with G_i protein bias, and β-arrestin with and without bias, respectively.[23,65] Interestingly, density maps of simulations starting from the inactive state show that fentanyl reaches more intermediate intracellular states than morphine, the latter presenting a larger density closer to the inactive crystal conformation[29] (Figure 4). This result may suppose an additional indication of the differences in efficacy observed between both ligands.[51−53] On the other hand, the possibility that the higher trend of fentanyl of generating intermediate states may facilitate the generation of receptor conformations more prone to β-arrestin binding is a speculation to be considered in further studies.

Morphine and Fentanyl Mediate Different Orthosteric Pocket Conformational Changes. To ascertain which conformational changes in the orthosteric pocket, induced or selected by morphine and fentanyl (see Figure 1), are most responsible for observed intracellular conformational differences, we performed an energetic analysis of residues in close contact with each ligand (Figure S8). Accordingly, from residues in close contact with both ligands (summarized in Table 1), fentanyl makes stronger energetic interaction with Asp56$^{N\text{-term}}$, Gln126$^{2.60}$, Cys219^{ECL2}, and Tyr328$^{7.43}$, whereas morphine makes stronger interactions with Tyr150$^{3.33}$ and Lys235$^{5.39}$ (Figure S8). Both ligands establish the highly energetic and conserved MOR-opiate salt bridge with Asp149$^{3.32}$, as previously identified in other studies.[5,7,19,29,30,45]

https://dx.doi.org/10.1021/acs.jcim.0c00890
J. Chem. Inf. Model. 2021, 61, 1251−1274

From a conformational perspective, we observe (i) H-bonds (either direct or water-mediated) between the ligand and Asp149$^{3.32}$ or Tyr150$^{3.33}$ and between residues Asp149$^{3.32}$ and Tyr328$^{7.43}$, (ii) specific χ1 dihedral angles of Asp149$^{3.32}$ and Met153$^{3.36}$ (directly determined by conformational changes of Tyr150$^{3.33}$), and (iii) specific χ2 dihedral angle selections of Gln126$^{2.60}$ and Lys235$^{5.39}$ sidechains (Figure 5 and Figures S9−S12). Taking these metrics one by one, morphine and fentanyl have both been described to make a highly conserved MOR-opiate electrostatic interaction with Asp149$^{3.32}$, a residue located on TM3.[5,7,19,29,30,45] In our MD simulations, this interaction between the ligand and Asp149$^{3.32}$ is highly energetically favorable with bound fentanyl but even greater with bound morphine, independent of the initial receptor state (average interaction energy of −78.1 or −94.9 kcal/mol, respectively, Figure S8). Despite this energetic difference between morphine and fentanyl, both ligands maintain a stable interaction (<4.5 Å) over three microseconds between their amine group and Asp149$^{3.32}$ (Figure 5 and Figure S9). In addition, Asp149$^{3.32}$ presents different χ1 dihedral angle conformations when morphine or fentanyl is bound in the hMOR (Figure 5 and Figure S9). Two different Asp149$^{3.32}$ conformations are observable in our MD simulations: (i) a *trans* conformation (χ1 dihedral angle >115.0°), predominantly induced in 5/6 trajectories with bound fentanyl (average frequency of 89.2%, Figure 5 and Figure S9), which positions the sidechain closer to TM2 and (ii) a *gauche*− conformation (χ1 dihedral angle <115.0°) induced by morphine in all trajectories (average frequency of 93.7%, Figure 5 and Figure S9), which positions the sidechain away from TM2. Similar to morphine-bound replicas, when the antagonist naltrexone is bound to the hMOR, an overall Asp149$^{3.32}$ *gauche*− conformation is induced, independent of the initial state of the receptor (Figure 5 and Figure S9). Under this condition, conformational change from *gauche*− to *trans* conformation is only observed in replica #3 starting from the inactive state at 2.2 μs. As a result of the *trans* conformation predominantly observed with bound fentanyl, Asp149$^{3.32}$ is within closer H-bonding distance with Tyr328$^{7.43}$ located on TM7.[46] Activated and fully active crystal structures[5,30] show closer Asp149$^{3.32}$−Tyr328$^{7.43}$ interaction distances than the inactive crystal structure[29] (3.2 and 3.4 Å, respectively), and this interaction also differs in our MD simulations with either bound morphine or fentanyl (Figure 5 and Figure S9). Throughout 4/6 trajectories with bound fentanyl, independent of the initial receptor state, Asp149$^{3.32}$−Tyr328$^{7.43}$ maintains a closer interaction (<4.5 Å) with an H-bond occupancy of 89.5% (36.1 SD, Figure 5 and Figure S9). Conversely, across all trajectories with bound morphine, only transient interactions between Asp149$^{3.32}$ and Tyr328$^{7.43}$ are observed with a H-bond occupancy of 24.1% (22.4 SD, Figure 5 and Figure S9). Similarly, the *gauche*− conformation overall selected when naltrexone is bound leads to an Asp149$^{3.32}$−Tyr328$^{7.43}$ H-bond occupancy of 41.1%, independent of the starting receptor state (19.5 SD, Figure 5 and Figure S9). These results are supported by the low H-bond occupancy observed when the antagonist naltrexone is bound into the orthosteric pocket of the receptor (Asp149$^{3.32}$−Tyr328$^{7.43}$ H-bond occupancy of 41.6% across all replicas, Figure 5), which, despite being in close contact with Tyr328$^{7.43}$ like fentanyl, presents larger Asp149$^{3.32}$−Tyr328$^{7.43}$ distances. Therefore, fentanyl mediates a stronger Asp149$^{3.32}$−Tyr328$^{7.43}$ H-bond than morphine in the orthosteric pocket.

In addition to Asp149$^{3.32}$−ligand interaction, greater energetic interactions can also be observed between Tyr150$^{3.33}$ and morphine with respect to bound fentanyl (average potential energy (P.E.) of −5.6 kcal/mol (2.4 SD) or − 1.9 kcal/mol (2.7 SD), respectively, Figure S8). Differences in the energetic landscape between fentanyl and morphine relate to their different scaffold, which presents a single oxygen group in the former (carbonyl group) and three oxygen groups in the latter (one ether and two hydroxyl groups, Figure 1). This distinction translates to a different H-bond occupancy (either direct or water-mediated) between Tyr150$^{3.33}$ and fentanyl or morphine with average occupancies of 32.2% (7.2 SD) or 89.2% (9.4 SD), respectively (Figure 5). In the case of the antagonist naltrexone, which presents a scaffold similar to morphine (Figure 1), it adopts a Tyr150$^{3.33}$−naltrexone H-bond occupancy of 56.1% (9.6 SD, Figure 5). Tyr150$^{3.33}$ and morphine or naltrexone hydroxyl/carbonyl groups are considered either donors or acceptors when evaluating Tyr150$^{3.33}$−ligand H-bond presence/absence. The higher H-bond occupancy between morphine and Tyr150$^{3.33}$ enhances upward axial movement of TM3 (Figure 3, Table S1, and Figure S5) and exerts a stabilizing effect in the bottom of the receptor orthosteric pocket, as observed with the conformation of Met153$^{3.36}$ (Figure 5 and Figure S10). In MD simulations starting from the activated state, independent of the agonist bound, the Met153$^{3.36}$ χ1 dihedral angle generally adopts a *gauche*− conformation (∼60.0°). Likewise, in MD simulations starting from the inactive state with bound morphine, Met153$^{3.36}$ *gauche*− conformation is selected with a frequency of 93.2% (8.8 SD, Figure 5 and Figure S10). However, when fentanyl is bound, alternative conformations of Met153$^{3.36}$ (χ1 > 90.0°) are more frequently induced with a frequency of 65.3% (4.9 SD, Figure 5 and Figure S10). Interestingly, in naltrexone-bound conditions, Met153$^{3.36}$ *gauche*− conformation is overall selected only with a frequency of 58.3% (24.5 SD, Figure 5 and Figure S10), which indicates that this residue conformationally fluctuates more with bound naltrexone than when fentanyl or morphine is bound in the hMOR, probably as a result of the direct contact naltrexone makes with this sidechain (Table 1 and Figure S3). Selection of χ1 *gauche*− appears to be associated with aforementioned active-like conformations of TM3 (Figure 3, Table S1, and Figure S5). This process can be linked with fentanyl-mediated TM6 activation where the receptor core undergoes reorganization and becomes more flexible. Once this transition ends, the stability of the core can be recovered, as indicated by trajectories starting from the activated state (Figure 5 and Figure S10). Conversely to the low H-bond occupancy between fentanyl and Tyr150$^{3.33}$ in TM3, which conditions the conformation of Met153$^{3.36}$, an energetically favorable interaction with Gln126$^{2.60}$ on TM2 is established with an average P.E. of −3.0 kcal/mol (4.4 SD). This contrasts with an unfavorable average P.E. of +2.7 kcal/mol (2.2 SD) displayed by morphine (Figure S8). Subsequently, Gln126$^{2.60}$ shows conformational differences when morphine or fentanyl is bound in the hMOR (Figure 5 and Figure S11). In general, two different Gln126$^{2.60}$ χ2 dihedral angles are observed in our MD simulations: (i) a *cis* and (ii) *trans* (∼300.0° and ∼ 180.0°, respectively). By using a threshold of ± 240°, Gln126$^{2.60}$ can be categorized according to these two conformations (Figure 5 and Figure S11). Although both conformations are observable with each ligand, its frequency is noticeably different from one to another. Systems with bound fentanyl predominantly induce

https://dx.doi.org/10.1021/acs.jcim.0c00890
J. Chem. Inf. Model. 2021, 61, 1251−1274

the *trans* conformation 86.0% of the time (10.5 SD, Figure 5 and Figure S11), which positions Gln126$^{2.60}$ toward the orthosteric pocket, allowing a three-way sidechain interaction with Tyr328$^{7.43}$ and Asp149$^{3.32}$ and supporting closer Asp−Tyr interaction (Figure 5 and Figure S13). By contrast, morphine selects the Gln126$^{2.60}$ *cis* conformation with a frequency of 80.5% (13.5 SD, Figure 5 and Figure S11), which positions it toward the membrane and negatively affects the Asp−Tyr interaction (Figure 5 and Figure S13). Similar to morphine, naltrexone selects the Gln126$^{2.60}$ *cis* conformation with a frequency of 87.3% (10.0 SD, Figure 5 and Figure S11).

Finally, Lys235$^{5.39}$−agonist interaction is the only one established between morphine and TM5 and is present at least 20.0% of the time in 5/6 trajectories (Table 1 and Figure S2). This interaction shows energetic differences between morphine and fentanyl with an average P.E. of +6.1 kcal/mol (6.9 SD) or +16.5 kcal/mol (3.8 SD), respectively (Figure S7). Similar to Tyr150$^{3.33}$, the Lys235$^{5.39}$ amino group establishes an interaction with any of morphine's oxygen groups (ether, hydroxyl groups #1 and #2) with a H-bond occupancy of 63.5% (13.2 SD) but generally avoids interaction with fentanyl's carbonyl group (H-bond occupancy of 7.2% (6.9 SD), Figure 5 and Figure S12). When naltrexone is bound, which shares a similar scaffold with morphine (Figure 1), Lys235$^{5.39}$ H-bonds naltrexone with an occupancy of 43.9% (18.6 SD). In this specific interaction, ligand oxygen groups are only considered as acceptors. Accordingly, Lys235$^{5.39}$ displays two different χ2 dihedral angles, either adopting a *cis* or *trans* conformation (∼300.0° or ∼ 180.0°, respectively) where a threshold of ± 240° can be used to categorize these two sidechain conformations (Figure 5 and Figure S12). Independent of the bound ligand, the *trans* conformation is the most commonly selected with the sidechain interacting with the extracellular solvent rather than with the ligand. However, different rates of *cis* conformation are induced between fentanyl, morphine, and naltrexone, with average percentages of 11.5% (5.1 SD), 38.0% (13.9 SD), and 40.0% (14.9 SD), respectively (Figure 4 and Figure S12). In this case, the *cis* conformation permits interaction with the bound ligand. This indicates that morphine mediates different conformational dynamics of Lys235$^{5.39}$ (Figure S13), which, accordingly, helps to stabilize the binding pose of morphine inside the orthosteric pocket of the receptor.

Conformational Changes of Trp295$^{6.48}$ Inducing Different Bottom-Orthosteric Pocket Receptor Interactions Are Relevant in TM5−TM6 Packing. During activation of the MOR, TM6 moves outward, which, together with conformational rearrangement of TM3, TM5, and TM7, creates solvation of the intracellular cavity[5] and conformational changes in specific residues on TM6, such as Trp295$^{6.48}$.[5] By classifying sidechain conformation by dihedral angles, *gauche*− (0−120°), *trans* (120−240°), or *gauche*+ (240−360°) in mMOR crystals, Trp295$^{6.48}$ χ2 changes from *gauche*− to *trans* to *gauche*+ in inactive, activated, and fully active crystals, respectively (values of 78.6°, 121.3°, and 342.9°, respectively). In our MD simulations, we observe two stable Trp295$^{6.48}$ conformations (Figure 6 and Figure S14): (i) an activated-like *trans* conformation at 225.6° (6.9 SD) and (ii) an inactive-like *gauche*− conformation at 97.1° (4.1° SD). We do not observe the *gauche*+ conformation probably because, due to computational limitations, we have not included an interacting G_i protein in our simulations. In all trajectories starting from the activated hMOR state, independent of the agonist bound, the

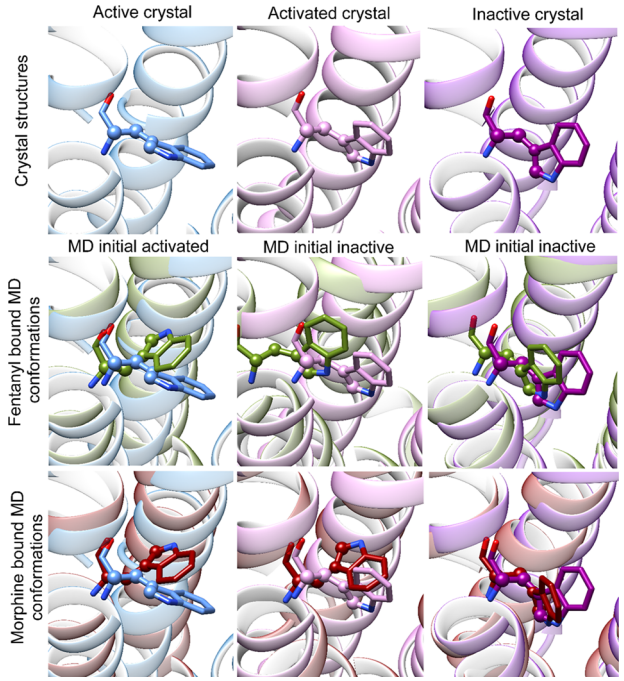

Figure 6. Trp295$^{6.48}$ conformational change in MD simulations with respect to MOR crystals. Comparison between different conformations of Trp295$^{6.48}$ (χ2 dihedral angle represented by spheres) of fully active, activated, and inactive crystals (salmon, blue and purple, respectively) and (i) representative MD-generated hMOR conformations with bound fentanyl (green, middle row) of replica #2 starting from the activated state, replicas #3 and #2 starting from the inactive state (from left to right, respectively) or, ii) with bound morphine (red, bottom row), replica #3 starting from the activated state, or replicas #1 and #2 starting from the inactive state (from left to right, respectively).

Trp295$^{6.48}$ *trans* conformation is stabilized within 1250 ns (Figures 6 and 7 and Figure S14). This enables a novel H-bond between Trp295$^{6.48}$ and Ala242$^{5.46}$ (sidechain amino group and backbone carbonyl group, respectively) with an average occupancy of 97.7% (1.1 SD), which is beneficial for maintaining active conformations of TM5 and TM6 (Figure 7). Conversely, all replicas starting from the inactive state with bound fentanyl, as well as replicas #2 and #3 where morphine is bound, select an inactive-like Trp295$^{6.48}$ *gauche*− conformation (Figure 6 and Figure S14). This conformation enables H-bonding with the adjacent residue on TM7, Asn330$^{7.45}$, which enhances TM6−TM7 interaction and avoids the interaction of this residue with water molecules, thus inhibiting TM6 activation (Figure 7). Interestingly, in replica #1 starting from the inactive state with bound morphine, the activated-like *trans* conformation is induced at 400 ns, which is the only replica in this category where the NPxxY motif yields an active-like conformation, observed from 200 ns onward (Figure S6). This enables sidechain−backbone Trp295$^{6.48}$−Ala242$^{5.46}$ H-bonding between TM5−TM6 with an occupancy of 68.0%, which assists TM5 activation after 500 ns (Figure S5), even though TM6 activation is not observed. Despite active-like conformations of the NPxxY motif being present in all replicas starting from the inactive state with bound fentanyl, only replica #3 transiently induces the *trans* conformation of Trp295$^{6.48}$ during the first 500 ns before returning to *gauche*− (Figure S14). This conformational change results in only 6% Trp−Ala H-bonding occupancy, but repeated sidechain

https://dx.doi.org/10.1021/acs.jcim.0c00890
J. Chem. Inf. Model. 2021, 61, 1251−1274

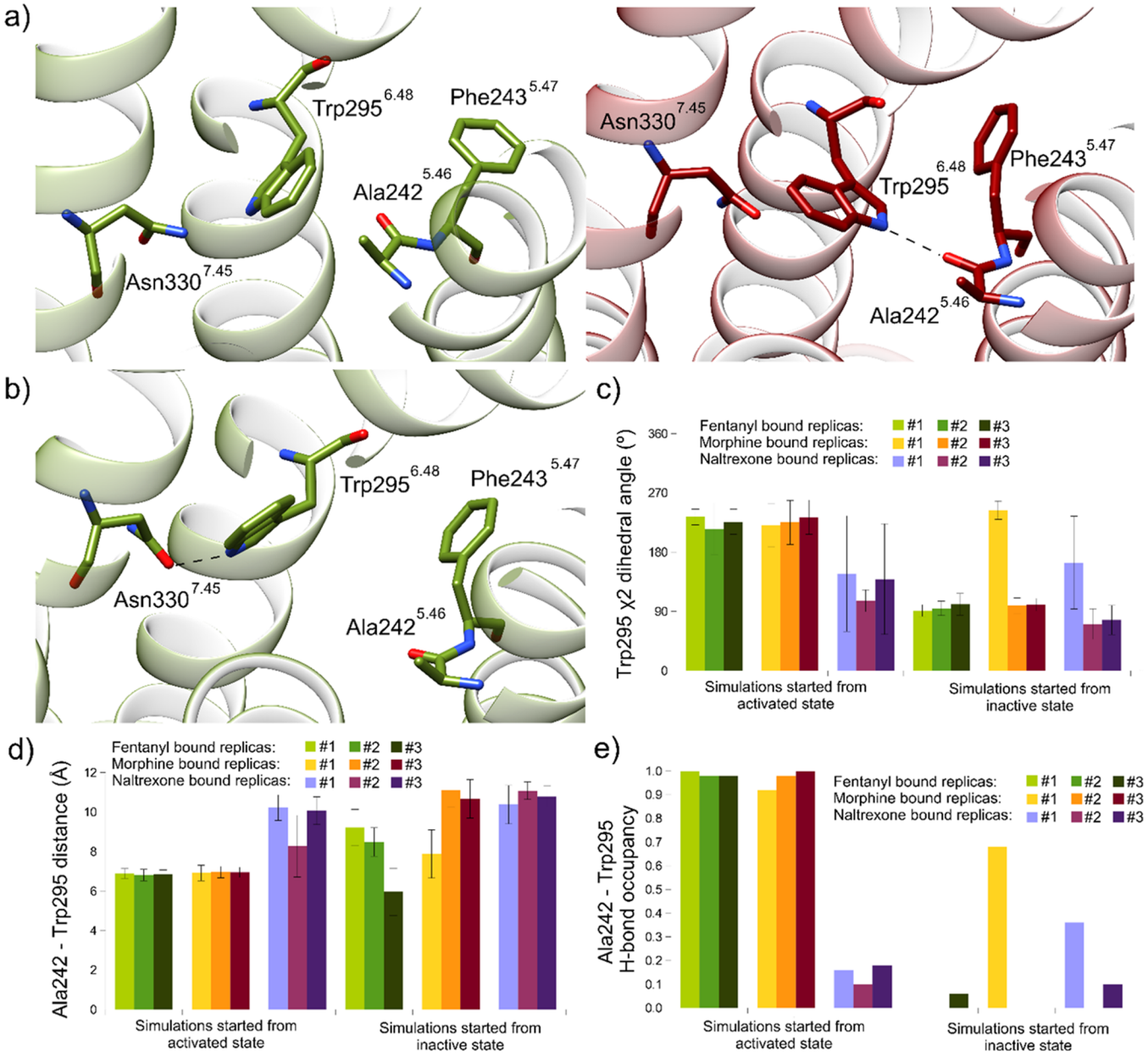

Figure 7. TM5−TM6 interaction in MD simulations: Trp295$^{6.48}$ and Ala242$^{5.46}$. MD-generated receptor structures showing the interaction of Trp295$^{6.48}$ with Ala242$^{5.46}$ or Asn330$^{7.45}$, in (a) replica #3 or #2 starting from inactive or activated states with bound fentanyl or morphine, respectively (left or right, green or red, respectively) or (b) replica #2 starting from the inactive state with bound fentanyl (green). (c−e) Per replica average (c) Trp295$^{6.48}$ χ2 dihedral angle, (d) Trp295$^{6.48}$−Ala242$^{5.46}$ distance, and (e) Trp295$^{6.48}$−Ala242$^{5.46}$ H-bond occupancy (shades of green, red, or purple for replicas #1−3 with bound fentanyl, morphine, or naltrexone, respectively).

switching is enough to trigger the gradual activation of TM6, which is observed more strongly later in this trajectory (Figure S6). Indeed, Trp295$^{6.48}$ and Ala242$^{5.46}$ mostly interact via hydrophobic contact for the rest of the trajectory (closest distance: 4.7 Å, Figure S14) rather than H-bonding because Trp295$^{6.48}$ remains in its *gauche*− conformation. This suggests that although bound morphine is capable of eliciting similar conformational changes in Trp295$^{6.48}$, switching from *gauche*− to *trans*, its effect can be different depending on other residues, such as Met153$^{3.36}$. In particular, it is noticeable in replica #3 with bound fentanyl that Met153$^{3.36}$ χ2 conformational switching occurs at the same time as Trp295$^{6.48}$ (Figures S10 and S13) with these switches in Met153$^{3.36}$ conformation becoming more frequent as TM6 moves outward. Despite these differences, closer interactions between Trp295$^{6.48}$ and Ala242$^{5.46}$ are observed with active-like conformations of TM5, TM6, and the NPxxY motif (Figure 7), which demonstrates the importance of rearrangements in TM5−TM6 packing. For comparison purposes, naltrexone-bound trajectories induced or selected *gauche*− conformations from respective activated or inactive states with percentages of 74.6 and 88.8%, respectively, with the closest Trp295$^{6.48}$−Ala242$^{5.46}$ distance of 8.4 Å achieved in control simulations starting from the inactive state. This distance, larger than that observed in fentanyl-bound trajectories, suggests a lack of TM5−TM6 packing, which favors the inactive state of the receptor. In addition, we observe different distributions between Asp149$^{3.32}$−Tyr328$^{7.43}$ H-bonding in the orthosteric pocket and Trp295$^{6.48}$−Ala242$^{5.46}$

https://dx.doi.org/10.1021/acs.jcim.0c00890
J. Chem. Inf. Model. 2021, 61, 1251−1274

interaction, where average Trp−Ala distances of 3.7 Å (1.8 SD) or 6.8 Å (3.0 SD) are reported when the Asp−Tyr H-bond is formed or broken, respectively (Figure S13). This demonstrates the interconnectivity of residue−residue interactions in the orthosteric pocket, which may have different implications for intracellular receptor conformations.

Intracellular Conformational Changes Correlate with Ligand-Specific Conformational Changes in the Receptor Orthosteric Pocket. In order to elucidate how ligand-specific orthosteric pocket conformational changes determine intracellular receptor conformations, we performed a number of statistical analyses (Figures S15 and S16) with respect to (in)activation of specific intracellular receptor metrics: TM3 upward-, TM5 inward-, TM6 outward-, and NPxxY motif inward-movement and Arg167$^{3.50}$−Thr281$^{6.34}$ distance. The chi-square (chi2) test was chosen to examine the association between these intracellular metrics and orthosteric pocket metrics: sidechain−sidechain Asp149$^{3.32}$−Tyr328$^{7.43}$, Lys235$^{5.39}$− or Tyr150$^{3.33}$−ligand, sidechain−backbone Trp295$^{6.48}$−Ala242$^{5.46}$ H-bond formation and Met153$^{3.36}$ *gauche*− conformation. The chi2 analyses involve two-way frequency tables of binary variables (presence/absence of H-bonds or Met153$^{3.36}$ *gauche*− conformation and active/inactive state of each intracellular metric, Figures S15 and S16). In addition, the potential association between the Trp295$^{6.48}$−Ala242$^{5.46}$ distance and active- or inactive-like state of the selected intracellular metrics was measured using Student's t-tests (Figure S16). All these statistical analyses were performed independently of the initial state of the receptor and the ligand bound. Our objective was not to find differences between ligands but to detect general mechanistic trends of receptor activation. Because we are combining data from different ligands and MD simulations with different starting states, we should take these tests as exploratory rather than confirmatory of the tested hypotheses. Nevertheless, the consistency found in the results suggests these analyses are valuable to realize the apparent relationships between the selected structural features. Chi2 tests show that differences exist between active- and inactive-like intracellular receptor conformations and Asp149$^{3.32}$−Tyr328$^{7.43}$, Tyr150$^{3.33}$−ligand, Lys235$^{5.39}$−ligand, Trp295$^{6.48}$−Ala242$^{5.46}$ H-bond formation and Met153$^{3.36}$ *gauche*− conformation (p < 0.05 in all cases, Figures S15 and S16). The absence of statistical significance was found for the association between Tyr150$^{3.33}$−ligand H-bond formation and the intracellular TM6 state (p = 0.051, Figure S15) and between Lys235$^{5.39}$−ligand H-bond formation and either TM3 or TM5 movements (p = 0.9 or 0.7, respectively, Figure S15). Interestingly, the fact that this last H-bond formation is not associated with movements of TM5 (Figure S15) suggests that Lys235$^{5.39}$ affects the position of the ligand in the orthosteric pocket, which in turn determines the conformation of other residues (such as Asp149$^{3.32}$), rather than directly transmitting the signal through TM5. Large chi2 values observed in the association between the sidechain−backbone Trp295$^{6.48}$−Ala242$^{5.46}$ H-bond and intracellular metrics (values between 252.7 and 582.9, which are extremely significant because 2 × 2 contingency tables contain 1 degree of freedom and significant P < 0.05 values are reached if chi2 > 3.841, Figure S16) highlight the relevance of this interaction in the (in)activation of the hMOR. Similarly, Student's t-tests show that the Trp295$^{6.48}$−Ala242$^{5.46}$ distance statistically differentiates between active and inactive TM3, TM5, TM6, and NPxxY motif conformational states and the Arg167$^{3.50}$−Thr281$^{6.34}$ distance state (p < 0.001 in all cases, Figure S16), showing overall Trp295$^{6.48}$−Ala242$^{5.46}$ closer distances in active- than inactive-like states. Close Trp295$^{6.48}$−Ala242$^{5.46}$ distances (see Methods), which are mainly attributed to helical rearrangement, enhance the establishment of hydrophobic contact between both residues. These results highlight the importance of these two residues becoming physically close irrespective of their H-bonding status.

Altogether, these results indicate that, independent of the ligand bound and the starting conformation of the receptor for MD simulations, mostly all orthosteric metrics studied in this study statistically reveal significant differences between active- and inactive-like states of the intracellular metrics used, thus establishing an (in)activation communication connection mechanism through the entire receptor. The differences found between agonists in their propensity to select or induce specific receptor conformations through these mechanistic structural features may explain the differences in efficacy observed experimentally.[27,51−53]

Internal Receptor Polar-Water Network Differs between Morphine and Fentanyl. A polar network mediated by water molecules has been described to be involved in signal transmission from the extracellular to the intracellular side of the mMOR.[5] An average water density map of the hMOR reveals differences in this network between activated/inactive states in morphine/fentanyl-bound MD simulations (Figure 8). As might be expected, the different molecular size and binding pose of fentanyl compared to morphine affects the number of water molecules that can enter

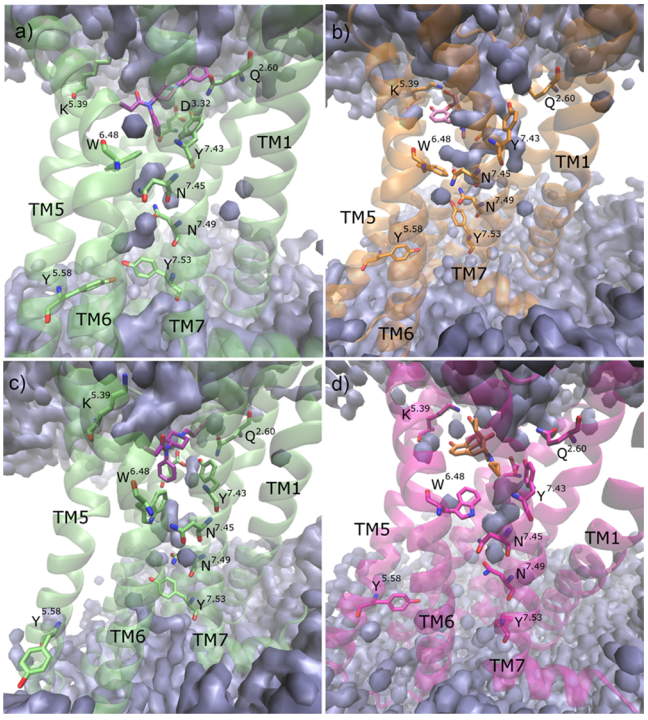

Figure 8. Polar water network in MD simulations. Comparison of the water network connecting extracellular and intracellular sides of the hMOR with bound fentanyl or morphine (green or orange, respectively). Receptor conformations from replicas #1 and #1 starting from the activated hMOR (snapshots at 2.4 μs and 3.0 μs, respectively) with (a) fentanyl and (b) morphine and replicas #3 and #1 starting from the inactive hMOR (pictures at 2.2 μs and 1.8 μs, respectively) with (c) fentanyl and (d) naltrexone.

https://dx.doi.org/10.1021/acs.jcim.0c00890
J. Chem. Inf. Model. 2021, 61, 1251−1274

the orthosteric pocket. Therefore, we observe more waters when morphine is bound than with fentanyl, independent of the initial receptor state (Figure 8). In terms of the receptor core or intracellular regions, two different water clusters can be identified: (i) between Trp295$^{6.48}$ and Asn330$^{7.45}$ on TM6 and TM7, respectively, and (ii) adjacent to the intracellular N$^{7.49}$PxxY$^{7.53}$ motif on TM7. In MD simulations with bound fentanyl, greater solvation is observed at both these regions, in particular near the NPxxY motif, which has previously been described as important for active conformations of the mMOR or class A GPCRs, in general.[5,79−81] This is consistent with stabilization of an active-like receptor conformation or receptor activation from the inactive state, which is observed in replica #3 with bound fentanyl (Figure 8). On the contrary, with bound morphine, these same water clusters are less pronounced, even with greater solvation in the orthosteric pocket, which suggests comparatively reduced receptor activation or increased destabilization of the active state. This is the case even when an active-like *trans* conformation of Trp295$^{6.48}$ is induced, which allows sidechain−backbone H-bonding with Ala242$^{5.46}$ (Figure 8), as observed in replica #1 when starting from the inactive state. Furthermore, in this same replica, despite corresponding activation of the NPxxY motif (Figure 3), the lack of TM6 conformational change as a whole allows fewer water molecules to access this region compared to simulations with bound fentanyl. In the same direction, when the antagonist naltrexone is bound, solvation of the two aforementioned regions is reduced even in simulations starting from the activated state, which facilitates hydrophobic interactions, TMD rearrangements, and inactivation of the receptor (Figure 8). This indicates that proper conformational movements of both TM6, most importantly through Trp295$^{6.48}$, and the NPxxY motif are necessary for formation of a water column in the receptor core, which is thought to be necessary for activation of the MOR.[5,79−81]

DISCUSSION

The recent spate of deaths from fentanyl and its derived compounds[51−53,56,57] raises special interest in how these high-efficacy agonists interact with the hMOR compared to lower-efficacy agonists such as morphine. Questions about potential differences between morphine- and fentanyl-based signaling lead to the need for better understanding of how these two ligands modulate MOR conformation and function and how this could instigate stronger responses from the receptor[51−53] or even stimulate different downstream pathways.[25,64] There are conflicting experimental data about whether fentanyl is a biased agonist or not. It was proposed through in vitro studies that fentanyl is more biased toward β-arrestin activation than morphine,[23,25,64] but the recent literature[65] did not find significant bias of neither fentanyl nor a collection of fentanyl analogues toward G_i protein or β-arrestin signaling pathways. Interestingly, opposite bias profiles were obtained for fentanyl depending on the model parameter used for bias quantification: G_i protein bias or β-arrestin bias when τ/K_A or τ parameters were respectively chosen.[64] MD simulations cannot give a definite answer to this problem. GPCR-dependent β-arrestin signaling involves the phosphorylation of particular serine or threonine residues at the intracellular regions of the receptor by GPCR kinases (GRKs). In a recent study on the dopamine D_1 receptor,[82] it was found that intracellular loop 3 (ICL3) phosphorylation affects arrestin binding and activation through various phosphorylation patterns, which direct the signaling to either one effector or another. This bar-coded phosphorylation signaling affects indirectly G protein coupling because arrestin- and G protein-coupled receptor populations coexist and the increase of one population decreases the other.[82] However, phosphorylation patterns may vary between GPCRs, in particular for the MOR. For this receptor, it was found that a single threonine (T180) in ICL2 is fundamental for agonist-dependent receptor phosphorylation and subsequent arrestin binding, activation, and signalling.[83] In the present study, the examination of MD simulations of the hMOR with either fentanyl or morphine bound did not find differences with respect to T180. It is worth noting that with present computational means, it is not possible to assess which active receptor conformations are more prone to be phosphorylated, which ultimately lead to β-arrestin signaling. However, at the timescales and starting models used, our MD simulations suggest the presence of a single common active-like receptor state stabilized by both morphine and fentanyl, in comparison to multiple conformations observed in other GPCRs such as the adenosine A2A receptor.[78] This leads us to consider an unbiased behavior of both morphine and fentanyl, where both ligands achieve a common active-like receptor state by differently activating ligand-specific conformations of the receptor. Nevertheless, it cannot be completely discarded that the higher propensity of fentanyl to induce receptor intermediate states could facilitate the generation of conformations predisposed to β-arrestin binding. In addition, it is worth noting that reliable quantification of biased agonism needs the use of proper parameters, and in this regard, the following has been proposed: the use of operational efficacy (τ) versus the transduction coefficient (τ/K_A) in the case of comparing ligands producing different maximum responses or, in other words, when partial agonism is present[64] or, moreover, the inclusion of constitutive receptor activity in the mathematical modeling in those cases where basal receptor response is observed.[17,84] On the contrary, other authors have applied the E_{max}/EC_{50} parameter for bias calculation of μ-opioid agonists.[65] Thus, it may happen that the mathematical models used for agonist bias quantification, in particular in those systems where pharmacological complexity either at the ligand (partial agonism) or receptor (constitutive activity) levels is present, may have permitted the occurrence of conflicting results in some cases. Nevertheless, a connection between functional experimental results yielded by ligands from particular receptors and the molecular interactions of these ligands with the residues in the receptor binding pocket is expected. The observed functional response is a consequence of molecular events that occur first within the receptor and are later propagated to the effector system.

The results obtained in this study greatly depend on the interactions established by morphine and fentanyl in the MOR orthosteric pocket, which to be properly determined requires a sufficiently accurate initial docking pose, as has been previously demonstrated in MD simulations of other GPCR-ligand complexes.[86] In this regard, our accurate docking of co-crystallized ligands (or their close analogues) gives us reason to have confidence in our docking protocol. We consider that, in order to properly characterize the efficacy of fentanyl and morphine in humans, it is important to study the hMOR instead of the mMOR, thus avoiding protein−ligand interactions with non-conserved residues. At the time our models were generated, only crystals of the activated[5] and inactive[29] mMOR were available. Models of activated or

https://dx.doi.org/10.1021/acs.jcim.0c00890
J. Chem. Inf. Model. 2021, 61, 1251−1274

inactive hMOR states were successfully validated by high conformational stability in MD simulations of the receptor and bound control ligands: BU-72 and naltrexone. However, a third mMOR crystal structure[30] was later released, which details the fully active receptor conformation coupled to human G_i protein. Despite not providing data of the β-arrestin signaling pathway, it supposes a novel point of reference for comparison with our MD simulations in terms of G_i protein signaling. Therefore, this crystal structure was used as an independent positive control, which, in addition to the use of co-crystallized BU-72-bound activated hMOR and naltrexone-bound inactive hMOR, allows us to quantify different conformational changes induced or selected in the hMOR by fentanyl or morphine. The question arises which is the proper reference state for the system. Both the apo receptor[87] and an antagonist-bound receptor may, in principle, be suitable for this purpose. We chose the latter condition because of the high stability of an antagonist-bound inactive receptor state, as well as the potential to deactivate an active receptor state to the inactive. However, utilizing the apo receptor to investigate the apparently low reported basal activity of the hMOR[85] is an interesting area for future study, in particular regarding potential allosteric modulation by anionic phospholipids as has been reported for other homologous class A GPCRs.[77,78,88] Under the simple framework of the two-state model of receptor activation: $R \overset{L}{\leftrightarrow} R^*$, with R and R^*, the inactive and active receptor states and L, the interconversion equilibrium constant $L = [R^*]/[R]$, the agonist intrinsic efficacy α can be seen either through the induction branch $AR \overset{\alpha L}{\leftrightarrow} AR^*$ or through the selection branches: $A + R \overset{K}{\leftrightarrow} AR$ and $A + R^* \overset{K/\alpha}{\longleftrightarrow} AR^*$ of the thermodynamic cycle, where K is the dissociation equilibrium constant. Thus, induction and selection approaches are equivalent in terms of intrinsic efficacy α within the context of four receptor species in equilibrium. However, the situation can be more complex when receptor states include ensembles of protein conformations. Conversion of AR into AR* may involve different intermediates with different kinetics. The kinetic component can be a limiting factor in some cases making more complex the correspondence between induction and selection approaches. Considering that the inactive receptor R is, normally, the major species in the absence of an agonist, it is expected that an agonist making "easier" the conversion of AR into AR* will reflect this molecular feature onto its pharmacological profile. Our simulations suggest that this could be the case in the comparison between morphine and fentanyl. Therefore, in the present study, receptor activation by either induction or selection of receptor active states has been considered. This has been possible because both inactive and active MOR structures were available. Therefore, when starting from a specific simulation initial state (activated or inactive hMOR) if the receptor achieves the opposite state (inactive- or active-like conformations, respectively) the induced-fit approach is followed, otherwise, if the initial state is preserved, we can state that a selection approach occurs. This makes the dynamic structural analysis more robust and reliable. It should be taken into account that because we are using receptor states obtained for particular ligands, there is a bias toward these states for those ligands structurally resembling the crystallized ones (BU72 and β-FNA). In this regard, the morphine binding pose is widely known[42,89,90] because of its similarity with the morphine-like scaffold of agonist BU-72 and antagonist β-FNA in the activated or inactive mMOR,[5,29] respectively. Conversely, the native fentanyl binding pose is still unclear, with previously proposed binding poses differing in their orientation,[26,90−96] and no consensus having been reached. Mutagenesis-based studies[46,97] first characterized the binding landscape of fentanyl and fentanyl derivatives involving Asp149$^{3.32}$, Tyr150$^{3.33}$, Asn152$^{3.35}$, Trp320$^{7.35}$, His321$^{7.36}$, and Tyr328$^{7.43}$. During the last two decades, the use of computational techniques has revealed new details in fentanyl binding, identifying different residues that might potentially interact.[25,26,91,96] Despite fentanyl being more prone to change in its initial conformation during our MD simulations compared to morphine, the same stable binding mode of fentanyl is reached in the first microsecond of all replicas, especially in the inactive receptor state. This is interesting because a recent report investigating fentanyl binding in MD simulations of the mMOR failed to obtain a stable binding pose in the inactive state unless sodium ions (a known negative allosteric modulator) were co-bound.[26] Such ions are not required in our study. As fentanyl and morphine are both agonists, it might be expected that they should favor binding of the activated state over the inactive; however, tight induced-fit of the activated crystal structure for its co-crystallized morphine-like agonist BU-72[5] appears to enable precise docking of morphine but partially hinders fentanyl. Conversely, the larger size of co-crystallized antagonist β-FNA in the inactive crystal[29] may favor a faster stabilization of fentanyl in this state compared to the activated one. Nevertheless, once stable ligand binding is reached within our MD simulations starting from activated or inactive states, morphine and fentanyl make different ligand−receptor interactions. In particular, morphine interacts more frequently with the N-terminus, TM5, TM6, and TM7, coming into contact with residues: Asp56$^{N\text{-ter}}$, Lys235$^{5.39}$, Ile298$^{6.51}$, Val302$^{6.55}$, Trp320$^{7.35}$, and Ile324$^{7.39}$, while fentanyl interacts with ECL2, TM2, and TM7, coming into contact with Gln126$^{2.60}$, Asn129$^{2.63}$, Val145$^{3.28}$, Cys219^{ECL2}, and Tyr328$^{7.43}$. However, there are similarities as both morphine and fentanyl interact with Ser57$^{N\text{-term}}$, Tyr150$^{3.33}$, and Asp149$^{3.32}$.

The different molecular scaffolds of morphine and fentanyl lead to different binding modes, which are associated with different conformational arrangements in the orthosteric pocket and which may be related to their different pharmacological efficacies. The widely described[5,7,17,29,30,45] electrostatic interaction with Asp149$^{3.32}$ has been observed as essential for binding of μ-opioid ligands, and the Asp149$^{3.32}$ conformation resulting from it plays a direct role in receptor (in)activation as shown by mutagenesis experiments.[26,48,49] Likewise, H-bonding between Asp149$^{3.32}$ and Tyr328$^{7.43}$ in the orthosteric pocket has been shown to be relevant for MOR activation.[26] Further experimental studies[26,46,95] have shown that Tyr328$^{7.43}$ has a significant effect on ligand potency and agonist-induced receptor activation, specifically for fentanyl, and is conserved and functional in δ- and κ-opioid receptors as demonstrated by mutagenesis.[98] Other mutagenesis studies have identified Tyr150$^{3.33}$ to be relevant for agonist binding affinity,[95,97] including fentanyl. In addition, mutation of the conserved residue Tyr139$^{3.33}$ in the κ-opioid receptor alters ligand potency.[98] Likewise, a recent mutagenesis study[99] has shown that Cys219^{ECL2} likely comes into contact with fentanyl and is relevant in its binding but does not affect receptor activation. This is an interesting result because it implies a molecular separation of the affinity and efficacy concepts,

https://dx.doi.org/10.1021/acs.jcim.0c00890
J. Chem. Inf. Model. 2021, 61, 1251−1274

which is difficult if not impossible to obtain by parameter estimation from functional studies as the estimated binding constants in operational models include the receptor activation component.[100] Therefore, our morphine binding pose is in accordance with previously described binding modes,[42,89,90] co-crystallized BU-72[5] and β-FNA,[29] and side-directed mutagenesis, which determined Val302$^{6.55}$ or Trp320$^{7.35}$ to be crucial for the decrease[101] or increase[29] of morphine affinity, respectively. Despite this, to our knowledge, no mutagenesis studies have been performed for residues: Asp56$^{N\text{-ter}}$, Lys235$^{5.39}$, and Ile324$^{7.39}$, even though they have been implicated in morphine binding before.[42,90] On the other hand, the fentanyl binding pose presented in our study, which presents protein−ligand interactions similar to those shown previously,[25,91] is in agreement with the first point mutation experiments[45,46,97] involving residues Asp149$^{3.32}$, Tyr150$^{3.33}$, and Tyr328$^{7.43}$ but not Asn152$^{3.35}$, Trp320$^{7.35}$, and His321$^{7.36}$. As far as we are aware, no experimental mutagenesis has been performed on Gln126$^{2.60}$ and Asn129$^{2.63}$, which we predict to interact with fentanyl. The relative stability of our observed binding poses of morphine and fentanyl, irrespective of receptor conformation, leads us to conclude that they are sufficiently accurate. As an extra validation of the fentanyl binding pose, we docked fentanyl to the new DAMGO-bound fully active crystal structure of the mMOR,[30] which might be expected to yield greater accuracy. This results in a similar docking pose to that obtained with our hMOR models and MD simulations (Figure S17), thus adding an extra layer of confidence.

Conformational dispositions in the orthosteric pocket lead to alteration of other receptor residues such as Met153$^{3.36}$ and Trp295$^{6.48}$, which assist receptor activation.[26,102,103] More specifically, different conformations of Met153$^{3.36}$ have been associated with a specific ligand-dependent microswitch for MOR β-arresting signaling.[25] Although in our results we have not found multiple active-like states, we observe different conformations of Met153$^{3.36}$ more frequently induced when either fentanyl or morphine is bound into the receptor orthosteric pocket. In addition, Trp295$^{6.48}$ has previously been observed to rotate during activation of the mMOR[26,103] and class A GPCRs, in general,[74] and has been commonly named a "toggle switch". Such "toggling" can result in different H-bonding between TM5, TM6, and TM7 and solvation of the receptor core.[26,103] In particular, it has been described that fentanyl stabilizes different rotameric states of Trp295$^{6.48}$ compared to morphine or the apo receptor.[26] In our study, we identify ligand-specific orthosteric pocket changes in (i) ligand interactions with Gln126$^{2.60}$, Asp149$^{3.32}$, Tyr150$^{3.33}$, and Lys235$^{5.39}$ including concomitant sidechain rotameric changes, (ii) interhelical Asp149$^{3.32}$−Tyr328$^{7.43}$ H-bonding, (iii) sidechain rotameric changes in Trp295$^{6.48}$ and Met153$^{3.36}$ (influenced by conformational change of Tyr150$^{3.33}$), and (iv) proximity and interhelical H-bonding between Trp295$^{6.48}$−Ala242$^{5.46}$ (influenced by conformational change in Trp295$^{6.48}$). In terms of how these conformational changes are connected, we observe that morphine and fentanyl engage with Asp149$^{3.32}$ via different *gauche*− or *trans* sidechain conformations, respectively. As *trans* Asp149$^{3.32}$ is within the H-bonding distance with Tyr328$^{7.43}$, as expected, we find higher Asp149$^{3.32}$−Tyr328$^{7.43}$ H-bond occupancy with bound fentanyl. Likewise, a *trans* sidechain conformation of Gln126$^{2.60}$, which is induced predominantly when fentanyl is bound, interacts with Tyr328$^{7.43}$, further stabilizing Asp149$^{3.32}$−Tyr328$^{7.43}$ H-bonding through a three-way sidechain interaction thus favoring receptor activation.[44,47] In comparison, the Gln126$^{2.60}$ *cis* sidechain conformation, predominantly selected by morphine, shows lower Asp149$^{3.32}$−Tyr328$^{7.43}$ H-bonding and less favorable receptor activation.[44,47] Differences in Gln126$^{2.60}$ conformation with fentanyl and morphine and their influence on Asp149$^{3.32}$−Tyr328$^{7.43}$ H-bonding may partly explain their difference in efficacy.[51−53,56,57] The sidechain conformation of Asp149$^{3.32}$, which is dictated by the different binding poses of morphine and fentanyl, is further dictated by different interactions the ligands make with Lys235$^{5.39}$. As both ligands contain an oxygen acceptor group(s), the sidechain amino group of Lys235$^{5.39}$ can theoretically interact with either. In relevant crystals, Lys235$^{5.39}$ covalently binds antagonist β-FNA,[29] does not interact with agonist BU-72,[5] and makes an H-bond with agonist DAMGO.[30] Differences in the molecular scaffold between ligands lead to higher Lys235$^{5.39}$−ligand H-bond occupancy with bound morphine, which results in different conformations of Lys235$^{5.39}$. Accordingly, Lys235$^{5.39}$−ligand H-bonding is related to enhanced stabilization of morphine relative to fentanyl in the orthosteric pocket, thus leading Asp149$^{3.32}$ to adopt a *gauche*− sidechain conformation when morphine is bound. Therefore, our results indicate that Asp149$^{3.32}$−Tyr328$^{7.43}$ H-bonding, previously described to be essential for MOR activation,[44,47] is determined by ligand interactions with Asp149$^{3.32}$ and Gln126$^{2.60}$ and by its position in the orthosteric pocket influenced by its interaction with Lys235$^{5.39}$.

Oxygen H-bond acceptor groups on morphine and fentanyl not only establish interactions with TM5 but also make H-bonds with Tyr150$^{3.33}$ on TM3, either directly or through a water molecule. Similar to Lys235$^{5.39}$, morphine has a higher Tyr150$^{3.33}$−ligand H-bond occupancy than fentanyl, which may enhance TM3 activation and exert a stabilizing effect on the receptor orthosteric pocket. This includes the crystal *gauche* sidechain conformation of Met153$^{3.36}$, which is largely induced in simulations starting from the activated state and when morphine is bound. This conformation stabilizes hydrophobic interactions that occur at the bottom of the orthosteric pocket restricting the transition from one state to the other. In this respect, signal transmission along TM3 from Tyr150$^{3.33}$ to Met153$^{3.36}$ of the hMOR is similar to that of other GPCRs such as the nociceptin receptor.[102] On the contrary, selection of the Met153$^{3.36}$ *trans* conformation by fentanyl when the receptor is in an inactive-like state suggests a destabilization of the hydrophobic interactions, which supports transition from an inactive receptor state to a more active one by disconnecting TM3 from TM6. These results indicate that fentanyl has a facility to change Met153$^{3.36}$ from an inactive to active-like conformation more frequently than morphine. In addition to Asp149$^{3.32}$−Tyr328$^{7.43}$ and Tyr150$^{3.33}$−ligand H-bonding and associated conformational change of Met153$^{3.36}$, the conformational toggling of Trp295$^{6.48}$ has previously been described in the activation of the MOR[26] and δ-opioid receptor.[104] The Trp295$^{6.48}$ sidechain also adopts different conformations in inactive,[29] activated,[5] and fully active crystals of the mMOR.[30] In our MD simulations with either bound morphine or fentanyl, Trp295$^{6.48}$ adopts an inactive-like *gauche* or an activated-like *trans* conformation depending on the receptor state and ligand bound. The *trans* position resembles the conformation observed in the fully active crystal structure,[30] adopting a perpendicular orientation to TM6 but

https://dx.doi.org/10.1021/acs.jcim.0c00890
J. Chem. Inf. Model. 2021, 61, 1251−1274

with the indole NH pointing toward TM5 instead of TM7. This conformation is in general agreement with a recent study implementing MD simulations of the mMOR with docked fentanyl but differs from those observed with docked morphine.[26] The reason for this discrepancy over morphine is unclear but could be due to differences between mouse and human receptor models or co-bound sodium ions, which might negate agonist activity.[26] In our simulations starting from the inactive hMOR, the *trans* conformation of Trp295$^{6.48}$ is only obtained twice, once with bound morphine and the other more transiently with fentanyl. This shows that activation of the hMOR, in particular TM6 conformational change, is a relatively difficult process to capture in a microsecond period. This contrasts with the relative ease of receptor activation observed in MD simulations of other class A GPCRs, such as CB1[77] or adenosine A2A.[78] In some respects, this fits with the low constitutive activity displayed by the hMOR in pharmacological experiments,[85] which suggests a highly stable inactive state. When Trp295$^{6.48}$ adopts the *trans* conformation, it allows interhelical H-bonding with Ala242$^{5.46}$, a position which has been shown to be relevant for TM5 flexibility in class A GPCRs.[81] Conversely, the *gauche* conformation of Trp295$^{6.48}$ H-bonds Asn330$^{7.45}$ when whole TM6 movement is not present and the distance between Trp295$^{6.48}$ and Ala242$^{5.46}$ is large. As a result, conformational change and activation of TM5 and TM6 are highly related to close Trp295$^{6.48}$−Ala242$^{5.46}$ interaction, either by H-bond formation or helical rearrangement. Together with Asp149$^{3.32}$−Tyr328$^{7.43}$ and Tyr150$^{3.33}$−ligand H-bonding, as well as Met153$^{3.36}$ conformational change in the receptor orthosteric pocket, these are the factors that most strongly govern intracellular receptor conformation and where differences between morphine and fentanyl are most clear.

In our MD simulations, conformational changes of TM helices differently occur with bound morphine or fentanyl. While morphine largely induces or selects conformational activation changes of TM3 and TM5, fentanyl more frequently achieved active-like conformations of TM6 and TM7. Conformational rearrangements of these TM helices are reflected in changes in specific intracellular regions such as Arg167$^{3.50}$−Thr281$^{6.34}$ interaction between TM3 and TM6 and the NPxxY motif on TM7. However, in the most part, we observe that the distance between Arg167$^{3.50}$ and Thr281$^{6.34}$ and conformation of the NPxxY motif remain constant when the receptor is already in the activated state with bound fentanyl or morphine, which means that both agonists generally sustain the active receptor state, which is consistent with their agonist character. However, activation of the receptor from the inactive state through breakage of Arg167$^{3.50}$−Thr281$^{6.34}$ interaction and conformational change of the NPxxY motif is more frequently observed with bound fentanyl than with morphine. This suggests that fentanyl more strongly induces conformational changes in the NPxxY motif through enhanced Asp149$^{3.32}$−Tyr328$^{7.43}$ H-bonding and enables TM3−TM6 separation through disruption of Met153$^{3.36}$ conformation and Trp295$^{6.48}$−Ala242$^{5.46}$ transient H-bonding and further close contact. This may be indicative of its higher efficacy observed at the experimental level[51−53] and also reflects the allosteric communication that operates between the orthosteric pocket and intracellular regions of the hMOR. Nearly all orthosteric metrics analyzed in this study have shown statistically significant association with the state of intracellular metrics studied, independent of the ligand bound and receptor starting state. This communication has been proposed to operate, at least in part, through a polar network mediated by water molecules, which changes depending on the receptor state.[5,79−81] Here, we have identified two water clusters, which differ between active- and inactive-like states or between morphine/fentanyl bound systems: (i) intracellular solvation near the NPxxY region on TM7 and (ii) solvation in the receptor core between Asn330$^{7.45}$ and Trp295$^{6.48}$. In particular, the former has been described to occur during activation of the hMOR and class A GPCRs in general.[5,53,81] This is partly because TM6 conformational change involved in the transition from the inactive to near-active receptor state, as observed more with bound fentanyl, leads to greater solvation in intracellular receptor regions, including the NPxxY motif, as well as the receptor core near Trp295$^{6.48}$. On the contrary, the smaller size of morphine allows greater solvation of the orthosteric pocket, which may negatively affect its binding stability in the inactive receptor state. Furthermore, the energetic state of these waters and how fentanyl potentially displaces more of them in the orthosteric pocket relative to morphine can be the topic of future study.

In summary, our dynamics of the hMOR are determined by ligand binding to activated[5] and inactive[29] receptor models, based on mMOR crystal structures, including extracellular/intracellular loops and modeled N-termini. The recently published fully active mMOR cryo-EM structure[30] allows for an independent positive control of MD-generated receptor structures. In addition, MD simulations with the antagonist naltrexone bound represent a negative control that allows us to better describe differences between fentanyl and morphine. Likewise, the constitution of the geometry of our hMOR models is validated by the mutual ligand and receptor conformational stability in control systems with BU-72 or naltrexone bound, respectively, to activated or inactive states. Two different physically stable binding poses of morphine and fentanyl in the hMOR mediate different sets of protein−ligand interactions (in particular involving Gln126$^{2.60}$, Lys235$^{5.39}$, Asp149$^{3.32}$, Lys235$^{5.39}$, and Tyr150$^{3.33}$), which differentially change orthosteric pocket conformation (in particular Asp149$^{3.32}$−Tyr328$^{7.43}$ H-bonding, Met153$^{3.36}$ orientation, and Trp295$^{6.48}$−Ala242$^{5.46}$ interaction). These result in different intracellular TM3, TM5, TM6, and TM7 conformational changes, including movement of the NPxxY motif and Arg167$^{3.50}$−Thr281$^{6.34}$ separation. Fentanyl has a stronger effect on TM6 and TM7 conformation, while morphine preferentially affects TM3 and TM5. As conformational change in TM6 is critical for GPCR activation and G protein binding in particular, this likely explains the enhanced receptor activity elicited by fentanyl in vivo, which has 50−100-fold higher potency than morphine.[51−53,56,57] The structural insights gained in the present study can be used in future work with a spread of μ-opioid targeting drugs, to identify those interactions and conformational changes associated with particular ligand efficacy and the disjunction between signaling networks through the receptor, which probably determine the proficiency in modulation of the receptor intracellular pocket and G_i protein or β-arrestin recognition.

METHODS

Homology Modeling. The crystal structures of activated and inactive states of the mMOR (PDB ids: 5C1M[5] and 4DKL[29]) were used to model respective hMOR states using Chimera v1.11[105] and Modeller v9.16.[106] Non-native camelid

https://dx.doi.org/10.1021/acs.jcim.0c00890
J. Chem. Inf. Model. 2021, 61, 1251−1274

G protein mimetic nanobody Nb39 and T4L lysozyme fusion protein were removed from respective activated[5] and inactive[29] mMOR crystal structures, as well as co-crystallized opioids: BU-72[5] and β-FNA,[29] respectively. In order to homology model human wt-sequence (Uniprot ID: P35372)[107] hMOR models, respective activated[5] and inactive[29] mMOR crystal structures were used as templates and with renumbered sequences, so Gly52 was renumbered to Gly54, and so. Using Chimera[105] and the Dunbrack 2010 rotamer library,[108] sidechain modifications were performed on S55R, H56D, Q61P, V68I, N139T, V189I, and I308V, which correspond to nonconserved residues between species. The most probable rotamer with the fewest steric clashes was chosen in each instance. Using Modeller,[106] noncrystallized segments of the inactive hMOR N-terminus (residues Gly54 to Ile73), inactive hMOR intracellular loop 3 (ICL3; residues Val264 to Lys271), and activated hMOR C-terminus (residues Arg347 to Ile354) were homology modeled using the other receptor structure as a template. Subsequently, activated and inactive hMOR models were energy-minimized in the AMBER14SB force-field[109] using Chimera in vacuum conditions[105] to optimize internal interactions.

Ligand Docking. The structures of three ligands of interest for the present study, morphine and fentanyl, and negative control naltrexone, were extracted from Pubchem[110] and docked in activated and inactive hMOR models using Autodock4.2.6.[111] Specifically, morphine, fentanyl, and naltrexone were prepared by respectively selecting their bioactive isomer, protonating their amino group (consistent with physiological pH), and assigning a net charge of +1 in order to correctly interact with Asp149$^{3.32}$. This particular protein−ligand interaction is in accordance with co-crystallized μ-opioid agonists (BU-72; DAMGO),[5,30] antagonist (β-FNA),[29] and related structural data.[91] In addition to the naltrexone-bound inactive state of the hMOR, for control purposes, co-crystallized BU-72 was re-docked into the activated hMOR state with its amino group protonated as other ligands. Docking grid points were extended to cover total orthosteric pocket volumes, respectively. The selected docked conformation of each ligand in each receptor state represents the top hit identified by the best predicted affinity, which also makes correct interaction with Asp149$^{3.32}$. Subsequent docked ligand−receptor complexes were energy-minimized in the AMBER14SB force-field[109] using Chimera[105] in vacuum conditions to optimize protein−ligand interactions.

MD System Setup. Two control systems, BU-72 bound to the activated hMOR and naltrexone bound to the inactive hMOR, and five different systems of interest were generated: morphine-bound activated and inactive hMOR, fentanyl-bound activated and inactive hMOR, and naltrexone-bound activated hMOR; each embedded separately into a POPC membrane using the CHARMM-GUI web-based interface[112] and solvated with TIP3P water molecules. All models were oriented in the membrane according to the OPM database[113] entry of the activated mMOR (id: 5c1m).[5] The disulfide bridge between Cys142$^{3.25}$ and Cys219^{ECL2} was maintained in all systems, and charge neutralizing ions (0.15 M KCl) were automatically introduced in order to make a net system charge of 0. CHARMM-GUI[112] automatically generated membrane, water, and protein parameters according to the CHARMM36 force-field[114] and ligand parameters in accordance with CHARMM General Force Field (CGenFF) v.1.0.0.[115]

MD Simulations. MD simulations of each hMOR system starting from either activated or inactive states with bound morphine, fentanyl, or naltrexone were performed in triplicate using the CHARMM36 force-field[114] with ACEMD[116] on specialized GPU-computer hardware. Each replica was energy-minimized for 2000 steps followed by 28 ns of equilibration at 300 K and 1 atm, with positional harmonic restraints on protein and ligand heavy atoms progressively released over the first 8 ns of equilibration and thereafter continued without restraints. This was followed with an unbiased continuous production run under the same conditions for 3 μs for each replica. In addition, the control hMOR system with bound BU-72 was run in duplicate for 2 μs after the same energy-minimization and equilibration process as systems of interest, making a total additive simulation time of 58 μs.

MD Simulation Analysis. In order to evaluate activated and inactive hMOR model accuracy, we respectively analyzed the conformational stability of the receptor helical domain and co-crystallized ligand BU72 or naltrexone (substituted for co-crystallized β-FNA) making use of RMSD measurements with VMD software v1.9.2.[117] Analysis of the three microseconds of each trajectory with bound morphine, fentanyl, or naltrexone (including control replicas of the naltrexone-bound inactive state) was performed using VMD[117] with the following protocol: (i) ligand stability in inactive and activated hMOR models and (ii) analysis of respective stable binding poses; (iii) comparison between ligand-mediated hMOR orthosteric pocket conformational changes and their correlation with (iv) TM helical movement; (v) intracellular receptor conformational state and (vi) conformational changes of the rest of the receptor; (vii) water-network differences associated with different receptor states. Evaluation of conformational stability was measured by the analysis of the two last microseconds of each replica of the systems generated, whereas residue-specific conformational changes were studied considering the entire simulation time-period. In detail, RMSD measurements of fentanyl or morphine in their respective MD simulations were used to monitor ligand stability. In addition, all fentanyl, morphine, and naltrexone conformations achieved during respective trajectories were classified into five different clusters using a cutoff of 2.0 Å using VMD Clustering Tool.[117] A list of residues that came into contact with either morphine or fentanyl (<3.5 Å) in each replica of each system and their frequency were extracted making use of a smoothing/averaging TCL script[118] executed in VMD.[117] Electrostatic, van der Waals, and hydrophobic interactions between the ligand and residues with frequencies ≥20.0% in two or more replicas were analyzed for energetics using NAMD Energy plugin[119] v1.4 within VMD.[117] RMSD analysis of the hMOR TM domain was performed with respect to respective receptor starting conformation or with the fully active crystal[30] to assess receptor stability or (in)activation. A threshold of ± 3.5 Å from the initial receptor state as well as activated and inactive crystal conformational divergence from fully active crystal[30] was used to determine significant receptor conformational changes. Intracellular receptor conformational changes associated with activation/deactivation were analyzed by making use of VMD[117] in terms of movement with respect to the protein center of (i) TM3, (ii) the intracellular tip of TM5, (iii) the intracellular tip of TM6, and (iv) the NPxxY motif on TM7, in addition to (v) distance measurement between alpha carbons of residues Arg167$^{3.50}$ and Thr281$^{6.34}$. TM3 upward axial movement was measured by z axis offset difference between

https://dx.doi.org/10.1021/acs.jcim.0c00890
J. Chem. Inf. Model. 2021, 61, 1251−1274

TM3 and the protein center of mass (COM). Helix tips were defined according to the second and third-last intracellular helical turns (TM5: residues 251−261, TM6: 274−284) and distances measured relative to the protein COM. Taking in consideration differences between crystal structures[5,29,30] in their positions of TM3, TM5, and TM6 as well as MD simulations with the antagonist naltrexone bound, relevant internal distances measured were normalized with respect to the inactive crystal,[29] with respective distance thresholds of +0.3, −0.8, and + 1.7 Å used to classify active or inactive helix conformations. Active- or inactive-like conformations of intracellular metrics such as the NPxxY motif and Arg167$^{3.50}$−Thr281$^{6.34}$ interaction were defined by distance from the protein COM (using −0.8 Å threshold) or by +10.0 Å for Arg167$^{3.50}$−Thr281$^{6.34}$ inter-residue distance. Residues showing differences in their P.E. of interaction between bound fentanyl and morphine were analyzed according to (i) sidechain χ1 dihedral angle; (ii) χ2 dihedral angle; (iii) P.E. of interaction with nearby residues; (iv) distribution with respect to conformational changes of other residues; and (v) correlation with intracellular receptor conformational changes. Sidechain dihedral angles were classified according to a threshold between predominantly observed χ1 and χ2 dihedral angle conformations. Thus, a ± 115.0° value was used as a threshold for classifying Asp149$^{3.32}$ χ1 dihedral angle conformation (*gauche* and *trans* conformations), ± 90.0° threshold for the Met153$^{3.36}$ χ1 dihedral angle (*gauche* or alternative conformations), and ± 240.0° threshold for Lys235$^{5.39}$ and Gln126$^{2.60}$ χ2 dihedral angles (predominant *cis* and *trans* conformations of 300.0° and 180.0°, respectively). Electrostatic intersidechain or ligand−sidechain interactions were specified according to ± 4.5 Å distance threshold. H-bonding between morphine, fentanyl, or naltrexone with Asp149$^{3.32}$ was selected according to a threshold of ± 2.5 Å. Distances/H-bonding was measured between (i) fentanyl, morphine, or naltrexone amino groups and Asp149$^{3.32}$ gamma carbon (considered as the center of the Asp149$^{3.32}$ carboxylate group), (ii) fentanyl, morphine, or naltrexone oxygen acceptor/donor atoms (a single carbonyl group in the former or one ether and two hydroxyl groups in morphine or one ether, one hydroxyl group and one carbonyl group in naltrexone) and the Tyr150$^{3.33}$ hydroxyl group or the Lys235$^{5.39}$ amino group, (iii) Asp149$^{3.32}$ gamma carbon and the Tyr328$^{7.43}$ hydroxyl group, and (iv) the Trp295$^{6.48}$ indole NH group and the Ala242$^{5.46}$ backbone carbonyl group. Distance between residues Trp295$^{6.48}$ and Ala242$^{5.46}$ was measured between their respective sidechain COMs. Water density maps were created using VolMap within VMD[117] by calculating the weighted atomic density of water molecules averaged over the last two microseconds of each MD replica.

Statistical Analysis. Chi-square (Chi2) and Student's t-test statistical analyses were performed to assess the statistical significance of the potential association between orthosteric pocket metrics (sidechain−sidechain Asp149$^{3.32}$−Tyr328$^{7.43}$, Tyr150$^{3.33}$−ligand, Lys235$^{5.39}$−ligand, and sidechain−backbone Trp295$^{6.48}$−Ala242$^{5.46}$ H-bond presence or absence, Met153$^{3.36}$ *gauche* conformation selection, or Trp295$^{6.48}$−Ala242$^{5.46}$ distance, respectively) with the intracellular conformations achieved (active- or inactive-like conformation of TM3, TM5, TM6, NPxxY, and Arg167$^{3.50}$−Thr281$^{6.34}$ distance). To perform these analyses, we used 50 representative snapshots of each replica, extracted every 40 ns of the last two microseconds of respective trajectories, independent of the initial state of the receptor or the ligand bound, thus making a total sample of 900 receptor−ligand conformations. This sample was considered sufficient to construct two-way contingency tables to evaluate the Chi2 score and to perform Student's t-test analysis for exploring general mechanistic trends. $P < 0.05$ was considered statistically significant. IBM SPSS Statistics 20.0.0 was used for statistical analyses.

■ ASSOCIATED CONTENT

Supporting Information

The Supporting Information is available free of charge at https://pubs.acs.org/doi/10.1021/acs.jcim.0c00890.

(Figures S1−S17) Stability of BU-72 bound in the activated hMOR model during control MD simulations; morphine, fentanyl, and naltrexone conformational clustering and RMSD in MD simulations; proportion of residues in close contact with morphine, fentanyl, and naltrexone in MD simulations; entire TMD receptor conformational change; TM helix movement with respect to the protein center in MD simulations; intracellular Arg167$^{3.50}$−Thr281$^{6.34}$ distance in MD simulations; average potential energy per replica of protein−ligand and sidechain−sidechain interactions in MD simulations; fentanyl docking in active MOR crystal structures; statistical analyses; distribution of orthosteric pocket conformational changes; and (Table S1) average and SD of metrics mentioned in the text (PDF)

■ AUTHOR INFORMATION

Corresponding Authors

James A. R. Dalton − *Laboratory of Molecular Neuropharmacology and Bioinformatics, Unitat de Bioestadística and Institut de Neurociències, Universitat Autònoma de Barcelona, 08193 Bellaterra, Spain; Unitat de Neurociència Traslacional, Parc Taulí Hospital Universitari, Institut d'Investigació i Innovació Parc Taulí (I3PT), Institut de Neurociències, Universitat Autònoma de Barcelona, 08193 Bellaterra, Spain; Instituto de Salud Carlos III, Centro de Investigación Biomédica en Red de Salud Mental, CIBERSAM, 28029 Madrid, Spain*; Email: James.Dalton@uab.es

Jesús Giraldo − *Laboratory of Molecular Neuropharmacology and Bioinformatics, Unitat de Bioestadística and Institut de Neurociències, Universitat Autònoma de Barcelona, 08193 Bellaterra, Spain; Unitat de Neurociència Traslacional, Parc Taulí Hospital Universitari, Institut d'Investigació i Innovació Parc Taulí (I3PT), Institut de Neurociències, Universitat Autònoma de Barcelona, 08193 Bellaterra, Spain; Instituto de Salud Carlos III, Centro de Investigación Biomédica en Red de Salud Mental, CIBERSAM, 28029 Madrid, Spain*; orcid.org/0000-0001-7082-4695; Email: Jesus.Giraldo@uab.es

Author

Adrián Ricarte − *Laboratory of Molecular Neuropharmacology and Bioinformatics, Unitat de Bioestadística and Institut de Neurociències, Universitat Autònoma de Barcelona, 08193 Bellaterra, Spain; Unitat de Neurociència Traslacional, Parc Taulí Hospital Universitari, Institut d'Investigació i Innovació Parc Taulí (I3PT), Institut de Neurociències, Universitat Autònoma de Barcelona, 08193 Bellaterra, Spain; Instituto de Salud Carlos III, Centro de*

Investigación Biomédica en Red de Salud Mental, CIBERSAM, 28029 Madrid, Spain

Complete contact information is available at: https://pubs.acs.org/10.1021/acs.jcim.0c00890

Funding

This project has received funding from the European Union's Horizon2020 research and innovation programme under grant agreement No 848068 and from Ministerio de Ciencia, Innovación y Universidades (Spain) under grant agreement SAF2017-87199-R. This publication reflects only the authors' view, and the European Commission is not responsible for any use that may be made of the information it contains.

Notes

The authors declare no competing financial interest.

REFERENCES

(1) Steglitz, J.; Buscemi, J.; Ferguson, M. J. The future of pain research, education, and treatment: a summary of the IOM report "Relieving pain in America: a blueprint for transforming prevention, care, education, and research". *Transl. Behav. Med.* **2012**, *2*, 6−8.

(2) Breivik, H.; Collett, B.; Ventafridda, V.; Cohen, R.; Gallacher, D. Survey of chronic pain in Europe: prevalence, impact on daily life, and treatment. *Eur. J. Pain.* **2006**, *10*, 287−333.

(3) O'Brien, T.; Christrup, L. L.; Drewes, A. M.; Fallon, M. T.; Kress, H. G.; McQuay, H. J.; Mikus, G.; Morlion, B. J.; Perez-Cajaraville, J.; Pogatzki-Zahn, E.; Varrassi, G.; Wells, J. C. European Pain Federation position paper on appropriate opioid use in chronic pain management. *Eur. J. Pain.* **2017**, *21*, 3−19.

(4) Wang, J. B.; Johnson, P. S.; Persico, A. M.; Hawkins, A. L.; Griffin, C. A.; Uhl, G. R. Human mu opiate receptor. cDNA and genomic clones, pharmacologic characterization and chromosomal assignment. *FEBS Lett.* **1994**, *338*, 217−222.

(5) Huang, W.; Manglik, A.; Venkatakrishnan, A. J.; Laeremans, T.; Feinberg, E. N.; Sanborn, A. L.; Kato, H. E.; Livingston, K. E.; Thorsen, T. S.; Kling, R. C.; Granier, S.; Gmeiner, P.; Husbands, S. M.; Traynor, J. R.; Weis, W. I.; Steyaert, J.; Dror, R. O.; Kobilka, B. K. Structural insights into μ-opioid receptor activation. *Nature* **2015**, *524*, 315−321.

(6) Roeckel, L. A.; Utard, V.; Reiss, D.; Mouheiche, J.; Maurin, H.; Robé, A.; Audouard, E.; Wood, J. N.; Goumon, Y.; Simonin, F.; Gaveriaux-Ruff, C. Morphine-induced hyperalgesia involves mu opioid receptors and the metabolite morphine-3-glucuronide. *Sci. Rep.* **2017**, *7*, 10406.

(7) Kapoor, A.; Martinez-Rosell, G.; Provasi, D.; de Fabritiis, G.; Filizola, M. Dynamic and kinetic elements of μ-opioid receptor functional selectivity. *Sci. Rep.* **2017**, *7*, 11255.

(8) Raehal, K. M.; Walker, J. K.; Bohn, L. M. Morphine side effects in β-arrestin 2 knockout mice. *J. Pharmacol. Exp. Ther.* **2005**, *314*, 1195−1201.

(9) DeWire, S. M.; Yamashita, D. S.; Rominger, D. H.; Liu, G.; Cowan, C. L.; Graczyk, T. M.; Chen, X. T.; Pitis, P. M.; Gotchev, D.; Yuan, C.; Koblish, M.; Lark, M. W.; Violin, J. D. A G protein-biased ligand at the μ-opioid receptor is potently analgesic with reduced gastrointestinal and respiratory dysfunction compared with morphine. *J. Pharmacol. Exp. Ther.* **2013**, *344*, 708−717.

(10) Schneider, S.; Provasi, D.; Filizola, M. How oliceridine (TRV-130) binds and stabilizes a μ-opioid receptor conformational state that selectively triggers G protein signaling pathways. *Biochemistry* **2016**, *55*, 6456−6466.

(11) FDA Approves New Opioid for Intravenous Use in Hospitals, Other Controlled Clinical Settings. FDA news release web site. https://www.fda.gov/news-events/press-announcements/fda-approves-new-opioid-intravenous-use-hospitals-other-controlled-clinical-settings (accessed Dec 3, 2020).

(12) OLINVYK (oliceridine) injection, for intravenous use, CII. Olinvyk web site. https://olinvyk.com/docs/OLINVYK_Final_Label_Ver%20002_Nov2020_1103.pdf (accessed Dec 3, 2020).

(13) Lambert, D.; Calo, G. Approval of oliceridine (TRV130) for intravenous use in moderate to severe pain in adults. *Br J Anaesth.* **2020**, *125*, e473−e474.

(14) Gurevich, V. V.; Gurevich, E. V. Biased GPCR signaling: Possible mechanisms and inherent limitations. *Pharmacol. Ther.* **2020**, *211*, 107540.

(15) Wingler, L. M.; Skiba, M. A.; McMahon, C.; Staus, D. P.; Kleinhenz, A. L. W.; Suomivuori, C. M.; Latorraca, N. R.; Dror, R. O.; Lefkowitz, R. J.; Kruse, A. C. Angiotensin and biased analogs induce structurally distinct active conformations within a GPCR. *Science* **2020**, *367*, 888−892.

(16) Kenakin, T.; Christopoulos, A. Signalling bias in new drug discovery: detection, quantification and therapeutic impact. *Nat. Rev. Drug Discovery* **2013**, *12*, 205−216.

(17) Hall, D. A.; Giraldo, J. A method for the quantification of biased signalling at constitutively active receptors. *Br. J. Pharmacol.* **2018**, *175*, 2046−2062.

(18) Gillis, A.; Sreenivasan, V.; Christie, M. J. Intrinsic efficacy of opioid ligands and its importance for apparent bias, operational analysis and therapeutic window. *Mol. Pharmacol.* **2020**, *119*, No. 119214.

(19) Manglik, A.; Lin, H.; Aryal, D. K.; McCorvy, J. D.; Dengler, D.; Corder, G.; Levit, A.; Kling, R. C.; Bernat, V.; Hübner, H.; Huang, X. P.; Sassano, M. F.; Giguère, P. M.; Löber, S.; Da, D.; Scherrer, G.; Kobilka, B. K.; Gmeiner, P.; Roth, B. L.; Shoichet, B. K. Structure-based discovery of opioid analgesics with reduced side effects. *Nature* **2016**, *537*, 185−190.

(20) Azzam, A. A. H.; McDonald, J.; Lambert, D. G. Hot topics in opioid pharmacology: mixed and biased opioids. *Br. J. Anaesth.* **2019**, *122*, e136−e145.

(21) Piekielna-Ciesielska, J.; Ferrari, F.; Calo, G.; Janecka, A. Cyclopeptide Dmt-[D-Lys-p-CF3-Phe-Phe-Asp]NH2, a novel G protein-biased agonist of the mu opioid receptor. *Peptides* **2018**, *101*, 227−233.

(22) Pasquinucci, L.; Turnaturi, R.; Calò, G.; Pappalardo, F.; Ferrari, F.; Russo, G.; Arena, E.; Montenegro, L.; Chiechio, S.; Prezzavento, O.; Parenti, C. (2S)-N-2-methoxy-2-phenylethyl-6,7-benzomorphan compound (2S-LP2): Discovery of a biased mu/delta opioid receptor agonist. *Eur. J. Med. Chem.* **2019**, *168*, 189−198.

(23) Schmid, C. L.; Kennedy, N. M.; Ross, N. C.; Lovell, K. M.; Yue, Z.; Morgenweck, J.; Cameron, M. D.; Bannister, T. D.; Bohn, L. M. Bias factor and therapeutic window correlate to predict safer opioid analgesics. *Cell* **2017**, *171*, 1165−1175.e13.

(24) Grim, T. W.; Acevedo-Canabal, A.; Bohn, L. M. Toward directing opioid receptor signaling to refine opioid therapeutics. *Biol. Psychiatry.* **2020**, *87*, 15−21.

(25) de Waal, P. W.; Shi, J.; You, E.; Wang, X.; Melcher, K.; Jiang, Y.; Xu, H. E.; Dickson, B. M. Molecular mechanisms of fentanyl mediated β-arrestin biased signaling. *PLoS Comput. Biol.* **2020**, *16*, No. e1007394.

(26) Lipiński, P. F. J.; Jarończyk, M.; Dobrowolski, J. C.; Sadlej, J. Molecular dynamics of fentanyl bound to μ-opioid receptor. *J. Mol. Model.* **2019**, *25*, 144.

(27) Morgan, M. M.; Christie, M. J. Analysis of opioid efficacy, tolerance, addiction and dependence from cell culture to human. *Br. J. Pharmacol.* **2011**, *164*, 1322−1334.

(28) Kelly, E. Efficacy and ligand bias at the μ-opioid receptor. *Br. J. Pharmacol.* **2013**, *169*, 1430−1446.

(29) Manglik, A.; Kruse, A. C.; Kobilka, T. S.; Thian, F. S.; Mathiesen, J. M.; Sunahara, R. K.; Pardo, L.; Weis, W. I.; Kobilka, B. K.; Granier, S. Crystal structure of the μ-opioid receptor bound to a morphinan antagonist. *Nature* **2012**, *485*, 321−326.

(30) Koehl, A.; Hu, H.; Maeda, S.; Zhang, Y.; Qu, Q.; Paggi, J. M.; Latorraca, N. R.; Hilger, D.; Dawson, R.; Matile, H.; Schertler, G. F. X.; Granier, S.; Weis, W. I.; Dror, R. O.; Manglik, A.; Skiniotis, G.;

Kobilka, B. K. Structure of the μ-opioid receptor-Gi protein complex. *Nature* **2018**, *558*, 547−552.
(31) Ballesteros, J. A.; Weinstein, H. [19] Integrated methods for the construction of three-dimensional models and computational probing of structure-function relations in G protein-coupled receptors. *Rec. Molar. Bio.* **1995**, *25*, 366−428.
(32) Filizola, M.; Devi, L. A. Structural biology: How opioid drugs bind to receptors. *Nature* **2012**, *485*, 314−317.
(33) Carroll, F. I.; Dolle, R. E. The discovery and development of the N-substituted trans-3,4-dimethyl-4-(3′-hydroxyphenyl)piperidine class of pure opioid receptor antagonists. *ChemMedChem* **2014**, *9*, 1638−1654.
(34) Yuan, Y.; Zaidi, S. A.; Elbegdorj, O.; Aschenbach, L. C.; Li, G.; Stevens, D. L.; Scoggins, K. L.; Dewey, W. L.; Selley, D. E.; Zhang, Y. Design, synthesis, and biological evaluation of 14-heteroaromatic-substituted naltrexone derivatives: pharmacological profile switch from mu opioid receptor selectivity to mu/kappa opioid receptor dual selectivity. *J. Med. Chem.* **2013**, *56*, 9156−9169.
(35) Fujita, W.; Gomes, I.; Devi, L. A. Revolution in GPCR signalling: opioid receptor heteromers as novel therapeutic targets: IUPHAR review 10. *Br. J. Pharmacol.* **2014**, *171*, 4155−4176.
(36) Lee, C. W.; Ho, I. K. Pharmacological profiles of oligomerized μ-opioid receptors. *Cell* **2013**, *2*, 689−714.
(37) Shang, Y.; LeRouzic, V.; Schneider, S.; Bisignano, P.; Pasternak, G. W.; Filizola, M. Mechanistic insights into the allosteric modulation of opioid receptors by sodium ions. *Biochemistry* **2014**, *53*, 5140−5149.
(38) Livingston, K. E.; Traynor, J. R. Disruption of the Na+ ion binding site as a mechanism for positive allosteric modulation of the mu-opioid receptor. *Proc. Nat. Acad. Sci. U. S. A.* **2014**, *111*, 18369−18374.
(39) Rasmussen, S. G.; Choi, H. J.; Fung, J. J.; Pardon, E.; Casarosa, P.; Chae, P. S.; Devree, B. T.; Rosenbaum, D. M.; Thian, F. S.; Kobilka, T. S.; Schnapp, A.; Konetzki, I.; Sunahara, R. K.; Gellman, S. H.; Pautsch, A.; Steyaert, J.; Weis, W. I.; Kobilka, B. K. Structure of a nanobody-stabilized active state of the β(2) adrenoceptor. *Nature* **2011**, *469*, 175−180.
(40) Ring, A. M.; Manglik, A.; Kruse, A. C.; Enos, M. D.; Weis, W. I.; Garcia, K. C.; Kobilka, B. K. Adrenaline-activated structure of β2-adrenoceptor stabilized by an engineered nanobody. *Nature* **2013**, *502*, 575−579.
(41) Kruse, A. C.; Ring, A. M.; Manglik, A.; Hu, J.; Hu, K.; Eitel, K.; Hübner, H.; Pardon, E.; Valant, C.; Sexton, P. M.; Christopoulos, A.; Felder, C. C.; Gmeiner, P.; Steyaert, J.; Weis, W. I.; Garcia, K. C.; Wess, J.; Kobilka, B. K. Activation and allosteric modulation of a muscarinic acetylcholine receptor. *Nature* **2013**, *504*, 101−106.
(42) Sounier, R.; Mas, C.; Steyaert, J.; Laeremans, T.; Manglik, A.; Huang, W.; Kobilka, B. K.; Déméné, H.; Granier, S. Propagation of conformational changes during μ-opioid receptor activation. *Nature* **2015**, *524*, 375−378.
(43) Huang, P.; Visiers, I.; Weinstein, H.; Liu-Chen, L. Y. The local environment at the cytoplasmic end of TM6 of the μ opioid receptor differs from those of rhodopsin and monoamine receptors: introduction of an ionic lock between the cytoplasmic ends of helices 3 and 6 by a L6.30(275)E mutation inactivates the μ opioid receptor and reduces the constitutive activity of its T6.34(279)K mutant. *Biochemistry* **2002**, *41*, 11972−11980.
(44) Dalton, J. A.; Lans, I.; Giraldo, J. Quantifying conformational changes in GPCRs: glimpse of a common functional mechanism. *BMC Bioinf.* **2015**, *16*, 124.
(45) Kaserer, T.; Lantero, A.; Schmidhammer, H.; Spetea, M.; Schuster, D. μ opioid receptor: novel antagonists and structural modeling. *Sci. Rep.* **2016**, *6*, No. 21548.
(46) Mansour, A.; Taylor, L. P.; Fine, J. L.; Thompson, R. C.; Hoversten, M. T.; Mosberg, H. I.; Watson, S. J.; Akil, H. Key residues defining the mu-opioid receptor binding pocket: a site-directed mutagenesis study. *J. Neurochem.* **1997**, *68*, 344−353.
(47) Xu, W.; Sanz, A.; Pardo, L.; Liu-Chen, L. Y. Activation of the mu opioid receptor involves conformational rearrangements of multiple transmembrane domains. *Biochemistry* **2008**, *47*, 10576−10586.
(48) Li, J. G.; Chen, C.; Yin, J.; Rice, K.; Zhang, Y.; Matecka, D.; de Riel, J. K.; DesJarlais, R. L.; Liu-Chen, L. Y. Asp147 in the third transmembrane helix of the rat μ opioid receptor forms ion-pairing with morphine and naltrexone. *Life Sci.* **1999**, *65*, 175−185.
(49) Befort, K.; Tabbara, L.; Bausch, S.; Chavkin, C.; Evans, C.; Kieffer, B. The conserved aspartate residue in the third putative transmembrane domain of the delta-opioid receptor is not the anionic counterpart for cationic opiate binding but is a constituent of the receptor binding site. *Mol. Pharmacol.* **1996**, *49*, 216−223.
(50) James, A.; Williams, J. Basic Opioid Pharmacology - An Update. *Br J Pain.* **2020**, *14*, 115−121.
(51) O'Donnell, J. K.; Halpin, J.; Mattson, C. L.; Goldberger, B. A.; Gladden, R. M. Deaths involving fentanyl, fentanyl analogs, and, U-47700 - 10 States, July-December 2016. *MMWR Morb. Mortal. Wkly. Rep.* **2017**, *16*, 1197−1202.
(52) Mounteney, J.; Giraudon, I.; Denissov, G.; Griffiths, P. Fentanyls: Are we missing the signs? Highly potent and on the rise in Europe. *Int. J. Drug Policy.* **2015**, *26*, 626−631.
(53) Vardanyan, R. S.; Hruby, V. J. Fentanyl-related compounds and derivatives: current status and future prospects for pharmaceutical applications. *Future Med. Chem.* **2014**, *6*, 385−412.
(54) Grissinger, M. Inappropriate prescribing of fentanyl patches is still causing alarming safety problems. *Pharm. Ther.* **2010**, *35*, 653−654.
(55) Schifano, F.; Chiappini, S.; Corkery, J. M.; Guirguis, A. Assessing the 2004-2018 fentanyl misusing issues reported to an international range of adverse reporting systems. *Front. Pharmacol.* **2019**, *10*, 46.
(56) Lyons, P. J.; Rivosecchi, R. M.; Nery, J. P.; Kane-Gill, S. L. Fentanyl-induced hyperalgesia in acute pain management. *J. Pain Palliat. Care Pharmacother.* **2015**, *29*, 153−160.
(57) Warner, M.; Trinidad, J. P.; Bastian, B. A.; Minino, A. M.; Hedegaard, H. Drugs most frequently involved in drug overdose deaths: United States, 2010-2014. *Natl. Vital Stat. Rep.* **2016**, *65*, 1−15.
(58) Skolnick, P. The Opioid Epidemic: Crisis and Solutions. *Annu. Rev. Pharmacol. Toxicol.* **2018**, *58*, 143−159.
(59) Verhamme, K. M. C.; Bohnen, A. M. Are We Facing an Opioid Crisis in Europe? *Lancet Public Health.* **2019**, *4*, e483−e484.
(60) Anselmi, L.; Jaramillo, I.; Palacios, M.; Huynh, J.; Sternini, C. Ligand-induced μ opioid receptor internalization in enteric neurons following chronic treatment with the opiate fentanyl. *J. Neurosci. Res.* **2013**, *91*, 854−860.
(61) Zheng, H.; Loh, H. H.; Law, P. Y. Beta-arrestin-dependent mu-opioid receptor-activated extracellular signal-regulated kinases (ERKs) translocate to nucleus in contrast to G protein-dependent ERK activation. *Mol. Pharmacol.* **2007**, *73*, 178−190.
(62) Mori, T.; Kuzumaki, N.; Arima, T.; Narita, M.; Tateishi, R.; Kondo, T.; Hamada, Y.; Kuwata, H.; Kawata, M.; Yamazaki, M.; Sugita, K.; Matsuzawa, A.; Baba, K.; Yamauchi, T.; Higashiyama, K.; Nonaka, M.; Miyano, K.; Uezono, Y.; Narita, M.. Usefulness for the combination of G protein- and β-arrestin-biased ligands of μ-opioid receptors: Prevention of antinociceptive tolerance. *Mol. Pain.* 2017.
(63) Kovoor, A.; Celver, J. P.; Wu, A.; Chavkin, C. Agonist induced homologous desensitization of μ-opioid receptors mediated by G protein-coupled receptor kinases is dependent on agonist efficacy. *Mol. Pharmacol.* **1998**, *54*, 704−711.
(64) Burgueño, J.; Pujol, M.; Monroy, X.; Roche, D.; Varela, M. J.; Merlos, M.; Giraldo, J. A complementary scale of biased agonism for agonists with differing maximal responses. *Sci. Rep.* **2017**, *7*, No. 15389.
(65) Vasudevan, L.; Vandeputte, M.; Deventer, M.; Wouters, E.; Cannaert, A.; Stove, C. P. Assessment of structure-activity relationships and biased agonism at the Mu opioid receptor of novel synthetic opioids using a novel, stable bio-assay platform. *Biochem. Pharmacol.* **2020**, *177*, No. 113910.

https://dx.doi.org/10.1021/acs.jcim.0c00890
J. Chem. Inf. Model. 2021, 61, 1251−1274

(66) Kalvass, J. C.; Olson, E. R.; Cassidy, M. P.; Selley, D. E.; Pollack, G. M. Pharmacokinetics and pharmacodynamics of seven opioids in P-glycoprotein-competent mice: assessment of unbound brain EC50,u and correlation of in vitro, preclinical, and clinical data. *J. Pharmacol. Exp. Ther.* **2007**, *323*, 346−355.
(67) Bobeck, E. N.; Haseman, R. A.; Hong, D.; Ingram, S. L.; Morgan, M. M. Differential development of antinociceptive tolerance to morphine and fentanyl is not linked to efficacy in the ventrolateral periaqueductal gray of the rat. *J. Pain.* **2012**, *13*, 799−807.
(68) Trescot, A. M.; Datta, S.; Lee, M.; Hansen, H. Opioid pharmacology. *Pain Physician.* **2008**, *11*, 133−153.
(69) Gillis, A.; Gondin, A. B.; Kliewer, A.; Sanchez, J.; Lim, H. D.; Alamein, C.; Manandhar, P.; Santiago, M.; Fritzwanker, S.; Schmiedel, F.; Katte, T. A.; Reekie, T.; Grimsey, N. L.; Kassiou, M.; Kellam, B.; Krasel, C.; Halls, M. L.; Connor, M.; Lane, J. R.; Schulz, S.; Christie, M. J.; Canals, M. Low intrinsic efficacy for, G protein activation can explain the improved side effect profiles of new opioid agonists. *Sci. Signaling* **2020**, *13*, No. eaaz3140.
(70) Changeux, J. P.; Edelstein, S. Conformational selection or induced fit? 50 years of debate resolved. *F1000 Biol. Rep.* **2011**, *3*, 19.
(71) Giraldo, J. Agonist induction, conformational selection, and mutant receptors. *FEBS Lett.* **2004**, *556*, 13−18.
(72) Lans, I.; Dalton, J. A. R.; Giraldo, J. Helix 3 acts as a conformational hinge in Class A GPCR activation: An analysis of interhelical interaction energies in crystal structures. *J. Struct. Biol.* **2015**, *192*, 545−553.
(73) Tehan, B. G.; Bortolato, A.; Blaney, F. E.; Weir, M. P.; Mason, J. S. Unifying family A GPCR theories of activation. *Pharmacol. Ther.* **2014**, *143*, 51−60.
(74) Rosenbaum, D. M.; Rasmussen, S. G.; Kobilka, B. K. The structure and function of G protein-coupled receptors. *Nature* **2009**, *459*, 356−363.
(75) Trzaskowski, B.; Latek, D.; Yuan, S.; Ghoshdastider, U.; Debinski, A.; Filipek, S. Action of molecular switches in GPCRs−theoretical and experimental studies. *Curr. Med. Chem.* **2012**, *19*, 1090−1109.
(76) Vogel, R.; Mahalingam, M.; Lüdeke, S.; Huber, T.; Siebert, F.; Sakmar, T. P. Functional role of the "ionic lock" - an interhelical hydrogen-bond network in family A heptahelical receptors. *J. Mol. Biol.* **2008**, *380*, 648−655.
(77) Díaz, Ó.; Dalton, J. A. R.; Giraldo, J. Revealing the mechanism of agonist-mediated cannabinoid receptor 1 (CB1) activation and phospholipid-mediated allosteric modulation. *J. Med. Chem.* **2019**, *62*, 5638−5654.
(78) Bruzzese, A.; Dalton, J. A. R.; Giraldo, J. Insights into adenosine A2A receptor activation through cooperative modulation of agonist and allosteric lipid interactions. *PLoS Comput. Biol.* **2020**, *16*, No. e1007818.
(79) Yuan, S.; Filipek, S.; Palczewski, K.; Vogel, H. Activation of G protein-coupled receptors correlates with the formation of a continuous internal water pathway. *Nat. Commun.* **2014**, *5*, 1−10.
(80) Tomobe, K.; Yamamoto, E.; Kholmurodov, K.; Yasuoka, K. Water permeation through the internal water pathway in activated GPCR rhodopsin. *PLoS One* **2017**, *12*, 1−14.
(81) Venkatakrishnan, A. J.; Ma, A. K.; Fonseca, R.; Latorraca, N. R.; Kelly, B.; Betz, R. M.; Asawa, C.; Kobilka, B. K.; Dror, R. O. Diverse GPCRs exhibit conserved water networks for stabilization and activation. *Proc. Natl. Acad. Sci. U. S. A.* **2019**, *116*, 3288−3293.
(82) Kaya, A. I.; Perry, N. A.; Gurevich, V. V.; Iverson, T. M. Phosphorylation barcode-dependent signal bias of the dopamine D1 receptor. *Proc. Natl. Acad. Sci. U. S. A.* **2020**, *117*, 14139−14149.
(83) Celver, J. P.; Lowe, J.; Kovoor, A.; Gurevich, V. V.; Chavkin, C. Threonine 180 is required for G protein-coupled receptor kinase 3- and beta-arrestin 2-mediated desensitization of the mu-opioid receptor in Xenopus oocytes. *J. Biol. Chem.* **2001**, *276*, 4894−4900.
(84) Zhou, B.; Hall, D. A.; Giraldo, J. Can Adding Constitutive Receptor Activity Redefine Biased Signaling Quantification? *Trends Pharmacol. Sci.* **2019**, *40*, 156−160.
(85) Seifert, R.; Wenzel-Seifert, K. Constitutive activity of G protein-coupled receptors: cause of disease and common property of wild-type receptors. *Naunyn-Schmiedeberg's Arch. Pharmacol.* **2002**, *366*, 381−416.
(86) Söldner, C. A.; Horn, A. H. C.; Sticht, H. A Metadynamics-Based Protocol for the Determination of GPCR-Ligand Binding Modes. *Int. J. Mol. Sci.* **2019**, *20*, 1970.
(87) Bruzzese, A.; Dalton, J. A. R.; Giraldo, J. Statistics for the analysis of molecular dynamics simulations: providing P values for agonist-dependent GPCR activation. *Sci. Rep.* **2020**, *10*, 19942.
(88) Bruzzese, A.; Gil, C.; Dalton, J. A. R.; Giraldo, J. Structural insights into positive and negative allosteric regulation of a G protein-coupled receptor through protein-lipid interactions. *Sci. Rep.* **2018**, *8*, 4456.
(89) Serohijos, A. W.; Yin, S.; Ding, F.; Gauthier, J.; Gibson, D. G.; Maixner, W.; Dokholyan, N. V.; Diatchenko, L. Structural basis for mu-opioid receptor binding and activation. *Structure* **2011**, *19*, 1683−1690.
(90) Berríos-Cárcamo, P.; Quintanilla, M. E.; Herrera-Marschitz, M.; Vasiliou, V.; Zapata-Torres, G.; Rivera-Meza, M. Racemic Salsolinol and its enantiomers act as agonists of the μ-Opioid receptor by activating the Gi protein-adenylate cyclase pathway. *Front. Behav. Neurosci.* **2017**, *10*, 253.
(91) Spahn, V.; Del Vecchio, G.; Labuz, D.; Rodriguez-Gaztelumendi, A.; Massaly, N.; Temp, J.; Durmaz, V.; Sabri, P.; Reidelbach, M.; Machelska, H.; Weber, M.; Stein, C. A nontoxic pain killer designed by modeling of pathological receptor conformations. *Science* **2017**, *355*, 966−969.
(92) Subramanian, G.; Paterlini, M. G.; Portoghese, P. S.; Ferguson, D. M. Molecular docking reveals a novel binding site model for fentanyl at the μ-opioid receptor. *J. Med. Chem.* **2000**, *43*, 381−391.
(93) Jarończyk, M.; Lipiński, P. F. J.; Dobrowolski, J. C.; Sadlej, J. The FMO analysis of the molecular interaction of fentanyl derivatives with the μ-opioid receptor. *Chem. Pap.* **2017**, *71*, 1429.
(94) Ellis, C. R.; Kruhlak, N. L.; Kim, M. T.; Hawkins, E. G.; Stavitskaya, L. Predicting opioid receptor binding affinity of pharmacologically unclassified designer substances using molecular docking. *PLoS One* **2018**, *13*, No. e0197734.
(95) Dosen-Micovic, L.; Ivanovic, M.; Micovic, V. Steric interactions and the activity of fentanyl analogs at the μ-opioid receptor. *Bioorg. Med. Chem.* **2006**, *14*, 2887−2895.
(96) Gentilucci, L.; Tolomelli, A.; De Marco, R.; Artali, R. Molecular docking of opiates and opioid peptides, a tool for the design of selective agonists and antagonists, and for the investigation of atypical ligand-receptor interactions. *Curr. Med. Chem.* **2012**, *19*, 1587−1601.
(97) Xu, H.; Lu, Y. F.; Partilla, J. S.; Zheng, Q. X.; Wang, J. B.; Brine, G. A.; Carroll, F. I.; Rice, K. C.; Chen, K. X.; Chi, Z. Q.; Rothman, R. B. Opioid peptide receptor studies, 11: involvement of Tyr148, Trp318 and His319 of the rat mu-opioid receptor in binding of mu-selective ligands. *Synapse* **1999**, *32*, 23−28.
(98) Yan, F.; Mosier, P. D.; Westkaemper, R. B.; Stewart, J.; Zjawiony, J. K.; Vortherms, T. A.; Sheffler, D. J.; Roth, B. L. Identification of the molecular mechanisms by which the diterpenoid salvinorin A binds to kappa-opioid receptors. *Biochemistry* **2005**, *44*, 8643−8651.
(99) Zhang, P.; Johnson, P. S.; Zöllner, C.; Wang, W.; Wang, Z.; Montes, A. E.; Seidleck, B. K.; Blaschak, C. J.; Surratt, C. K. Mutation of human mu opioid receptor extracellular "disulfide cysteine" residues alters ligand binding but does not prevent receptor targeting to the cell plasma membrane. *Brain Res. Mol. Brain Res.* **1999**, *72*, 195−204.
(100) Roche, D.; van der Graaf, P. H.; Giraldo, J. Have many estimates of efficacy and affinity been misled? Revisiting the operational model of agonism. *Drug Discovery Today* **2016**, *21*, 1735−1739.
(101) Sader, S.; Anant, K.; Wu, C. To probe interaction of morphine and IBNtxA with 7TM and 6TM variants of the human μ-opioid receptor using all-atom molecular dynamics simulations with an explicit membrane. *Phys. Chem. Chem. Phys.* **2018**, *20*, 1724−1741.

https://dx.doi.org/10.1021/acs.jcim.0c00890
J. Chem. Inf. Model. 2021, 61, 1251−1274

(102) Della Longa, S.; Arcovito, A. "In silico" study of the binding of two novel antagonists to the nociceptin receptor. *J. Comput.-Aided Mol. Des.* **2018**, *32*, 385−400.
(103) Fowler, C. B.; Pogozheva, I. D.; Lomize, A. L.; LeVine, H., 3rd; Mosberg, H. I. Complex of an active mu-opioid receptor with a cyclic peptide agonist modeled from experimental constraints. *Biochemistry* **2004**, *43*, 15796−15810.
(104) Tryoen-Tóth, P.; Décaillot, F. M.; Filliol, D.; Befort, K.; Lazarus, L. H.; Schiller, P. W.; Schmidhammer, H.; Kieffer, B. L. Inverse agonism and neutral antagonism at wild-type and constitutively active mutant delta opioid receptors. *J. Pharmacol. Exp. Ther.* **2005**, *313*, 410−421.
(105) Pettersen, E. F.; Goddard, T. D.; Huang, C. C.; Couch, G. S.; Greenblatt, D. M.; Meng, E. C.; Ferrin, T. E. UCSF Chimera–a visualization system for exploratory research and analysis. *J. Comput. Chem.* **2004**, *25*, 1605−1612.
(106) Webb, B.; Sali, A. Protein structure modeling with MODELLER. *Methods Mol. Biol.* **2014**, *1137*, 1−15.
(107) The UniProt Consortium. UniProt: the universal protein knowledgebase. *Nucleic Acids Res.* **2018**, *46*, 2699.
(108) Shapovalov, M. V.; Dunbrack, R. L., Jr. A smoothed backbone-dependent rotamer library for proteins derived from adaptive kernel density estimates and regressions. *Structure* **2011**, *19*, 844−858.
(109) Maier, J. A.; Martinez, C.; Kasavajhala, K.; Wickstrom, L.; Hauser, K. E.; Simmerling, C. ff14SB: Improving the accuracy of protein side chain and backbone parameters from ff99SB. *J. Chem. Theory Comput.* **2015**, *11*, 3696−3713.
(110) Kim, S.; Thiessen, P. A.; Bolton, E. E.; Chen, J.; Fu, G.; Gindulyte, A.; Han, L.; He, J.; He, S.; Shoemaker, B. A.; Wang, J.; Yu, B.; Zhang, J.; Bryant, S. H. PubChem substance and compound databases. *Nucleic Acids Res.* **2016**, *44*, 202−213.
(111) Morris, G. M.; Huey, R.; Lindstrom, W.; Sanner, M. F.; Belew, R. K.; Goodsell, D. S.; Olson, A. J. AutoDock4 and AutoDockTools4: Automated docking with selective receptor flexibility. *J. Comput. Chem.* **2009**, *30*, 2785−2791.
(112) Jo, S.; Kim, T.; Iyer, V. G.; Im, W. CHARMM-GUI: a web-based graphical user interface for CHARMM. *J. Comput. Chem.* **2008**, *29*, 1859−1865.
(113) Lomize, M. A.; Lomize, A. L.; Pogozheva, I. D.; Mosberg, H. I. OPM: orientations of proteins in membranes database. *Bioinformatics* **2006**, *22*, 623−625.
(114) Huang, J.; MacKerell, A. D. J. CHARMM36 all-atom additive protein force field: validation based on comparison to NMR data. *J. Comput. Chem.* **2013**, *34*, 2135−2145.
(115) Vanommeslaeghe, K.; Hatcher, E.; Acharya, C.; Kundu, S.; Zhong, S.; Shim, J.; Darian, E.; Guvench, O.; Lopes, P.; Vorobyov, I.; Mackerell, A. D., Jr. CHARMM General Force Field (CGenFF): A force field for drug-like molecules compatible with the CHARMM All-Atom Additive Biological Force Fields. *J. Comput. Chem.* **2010**, *31*, 671−690.
(116) Harvey, M. J.; Giupponi, G.; De Fabritiis, G. ACEMD: Accelerating biomolecular dynamics in the microsecond time scale. *J. Chem. Theory Comput.* **2009**, *5*, 1632−1639.
(117) Humphrey, W.; Dalke, A.; Schulten, K. VMD: visual molecular dynamics. *J. Mol Graphics.* **1996**, *14*, 33−38.
(118) Saam, J. Trajectory Smooth 1.1 TCL-script n.d. available at http://www.ks.uiuc.edu/ Research/vmd/script_library/scripts/trajectory_smooth/.
(119) Phillips, J. C.; Braun, R.; Wang, W.; Gumbart, J.; Tajkhorshid, E.; Villa, E.; Chipot, C.; Skeel, R. D.; Kalé, L.; Schulten, K. Scalable molecular dynamics with NAMD. *J. Comput. Chem.* **2005**, *26*, 1781−1802.

■ NOTE ADDED AFTER ASAP PUBLICATION

This paper was originally published ASAP on January 15, 2021. The TOC graphic and Figure 1 were replaced, and the paper was reposted on February 25, 2021.

https://dx.doi.org/10.1021/acs.jcim.0c00890
J. Chem. Inf. Model. 2021, 61, 1251−1274